Vienna University of Technology
Institute of Communications and Radio-Frequency Engineering

Master Thesis

# CPICH Power Optimization for MIMO HSDPA

Andreu Mateu Torrelló

executed for the purpose of obtaining the Master degree MASTEAM
Vienna March 2009

under the direction of

Projektass. Dipl.-Ing. Martin Wrulich
Univ.Prof. Dipl.-Ing. Dr.techn. Markus Rupp

# Abstract

The increasing demand of bandwidth from new network services has reached mobile technologies. Multiple-input multiple-output (MIMO) High-speed downlink packet access (HSDPA) can be the answer to this demand, being able to double the data rate of its predecessor single-input single-output (SISO) HSDPA. The optimization of mobile network is seen as an important issue from network operators, which see the opportunity to reduce costs by optimizing their networks through simulations. This thesis presents an overview of the main characteristics of enhanced MIMO HSDPA, describes the basic MIMO HSDPA link-level simulator we built and consequently focuses on the common pilot channel (CPICH) and its optimization. Furthermore, we derive a computationally efficient improvement, of the a link-measurement model utilized in a MIMO HSDPA system-level simulator, to take the effects of CPICH power variation into account.

# Acknowledgements

I would like to thank Martin Wrulich, who has guided me through this path called thesis, for his constant support and his optimistic approach, but especially for his patience.

I would also like to thank Professor Markus Rupp for giving me the opportunity to work in such a friendly environment, I felt like at home. My thank also goes to the whole institute of communications and radio-frequency engineering and my thesis students colleagues for helping me to clarify my ideas at any time during the day or night.

A la meva família, per donar-me suport en els moments més difícils, perquè tenir-vos al costat tot i que no sigueu a prop fa que em senti amb confiança per afrontar nous reptes.

Finally, I would to thank you, who helped me somehow at some point over the last 5 years, because without you I never would not have made it.

Palma de Mallorca
April 4, 2009

Andreu Mateu Torrelló

*for my mother*

# Contents

# List of Figures

# Glossary

| | |
|---|---|
| **3GPP** | 3rd generation parnership project |
| **AWGN** | Additive white gaussian noise |
| **BLER** | Block error ratio |
| **CPICH** | Common pilot channel |
| **CQI** | Channel quality indicator |
| **DCH** | Dedicated channel |
| **DS-CDMA** | Direct-sequence code division multiple access |
| **DSCH** | Downlink shared channel |
| **E-DCH** | Enhanced DCH |
| **FACH** | Forward access channel |
| **GSM** | Global system for mobile |
| **HARQ** | Hybrid-ARQ |
| **HS-DSCH** | High-speed downlink shared channel |
| **HS-PDSCH** | High-speed physical downlink shared channel |
| **HS-SCCH** | High-speed shared control channel |
| **HSDPA** | High-speed downlink packet access |
| **ISI** | Intersymbol interference |
| **ITU** | International telecommunication union |
| **LOS** | Line-of-sight |
| **LS** | Least squares |
| **MAI** | Multiple access interference |
| **MIMO** | Multiple-Input Multiple-Output |
| **MISO** | Multiple-input and single-output |

| | |
|---|---|
| **MMSE** | Minimum mean squared error |
| **MNO** | Mobile network operators |
| **MRC** | Maximum ratio combining |
| **MSE** | Mean square error |
| **NLOS** | Non-line-of-sight |
| **OVSF** | Orthogonal variable spreading factor |
| **P-CPICH** | Primary CPICH |
| **PDP** | Power delay profile |
| **RNC** | Radio network controllers |
| **RRM** | Radio resource management |
| **Rx** | receiver |
| **S-CCPCH** | Secondary common control physical channel |
| **S-CPICH** | Secondary CPICH |
| **SF** | Spreading factor |
| **SINR** | Signal-to-noise-and-interference ratio |
| **SISO** | Single-input single-output |
| **SNR** | Signal-to-noise ratio |
| **ST-MMSE** | Space-time minimum mean square error |
| **TFC** | Transport format combination |
| **TTI** | Transmission time interval |
| **Tx** | Transmitter |
| **UE** | User equipment |
| **UMTS** | Universal mobile telecommunications system |
| **WCDMA** | Wideband code division multiple access |

# 1. Introduction

## 1.1. MIMO HSDPA

Mobile radio communication represents one of the most persistent growing technology markets since the introduction of the Global System for Mobile communications (GSM). The Universal Mobile Telecommunications System (UMTS) was the evolution introducing Wideband Code Division Multiple Access (WCDMA) technology in mobile networks. Since then, the increasing availability of a broad range of new high-speed data services is fuelling demand for more bandwidth in order to improve the user experience.

High-Speed Downlink Packet Access (HSDPA) was introduced in Release 5 by the third Generation Parnership Project (3GPP) as the evolution of UMTS to give response to the new bandwidth demand. The natural evolution is HSPA+, which includes an enhanced version of HSDPA, doubles the data capacity and increases voice capacity by three times enabling operators to offer mobile broadband at even lower cost.

Multiple-Input Multiple-Output (MIMO), was introduced in Release 7, is one of the main techniques introduced to allow this increase of bandwidth. The optimization of MIMO HSDPA is on the mind of any operator wishing to launch this new system.

## 1.2. How important is the common pilot channel?

In HSDPA, as well as in UMTS, channel estimation is accomplished through the use of a signaling channel. Channel estimation is an essential part of a mobile system, because is the element that provides the knowledge of the channel coefficients which are crucial for the equalizer performance.

The Common Pilot CHannel (CPICH) is the signaling channel which aids the channel estimation. The variation of the CPICH power produces two main effects. On the one hand, the CPICH is used in the measurements for the handover and cell selection/reselection. The use of CPICH reception level at the terminal for handover

measurements has the consequence that, by adjusting the CPICH power level, the cell load can be balanced between different cells. Reducing the CPICH power causes part of the terminals to hand over to other cells, while increasing it invites more terminals to hand over to the cell, as well as to make their initial access to the network in that cell. On the other hand, the increase of the CPICH power derives better performance of the channel estimator, since the better the channel coefficients are estimated the higher the equalizer performance.

In this study we will focus on:

1. Enhancing the link-measurement model of the MIMO HSDPA system-level simulator in [5] to take the effects of CPICH power variation into consideration.
2. Determining an optimal CPICH power value for MIMO HSDPA networks.

## 1.3. Topics covered in this Master Thesis

To give a short overview, the thesis starts in Chapter 2 by presenting the principles of WCDMA and HSDPA, making a comparison on how the data is handled in HSDPA and UMTS. Chapter 3 covers in detail the design of a basic MIMO HSDPA link-level simulator. In Chapter 4 we discuss the importance of the combination of link-level and system-level simulators to provide a comprehensive study of the mobile network technologies and present the system-level model improvement. The CPICH power optimization is treated in Chapter 5. Additional material regarding some specific parts may be found in the Appendix.

# 2. HSDPA Basics

This chapter introduces the standardization of HSDPA in Section 2.1. In addition, the principles of WCDMA and HSDPA are presented in Sections 2.2 and 2.3 respectively.

## 2.1. Standardization

3GPP is the forum created at the ends of 1998 by US, Europe, Korea and Japan as the result of the desire to introduce a new single global standard for mobile communication based on WCDMA technology.

At the end of 1999 the first release was published, termed Release 99, containing the first full series of WCDMA specifications. Two years later, Release 4 specifications were issued. In the meantime it became obvious that some improvement for packet access would be needed [1].

A feasibility study for HSDPA was started in March 2000. The study was initially supported by Motorola and Nokia from the vendor side and BT/Cellnet, T-Mobil and NTT DoCoMo from the operator side. The study comprehended a set of improvements to be done over Release 99 specification. The main topics included physical layer retransmissions, BTS-based scheduling, adaptive coding and modulation, multi-antenna transmission and reception technology, called MIMO, as well as fast cell selection.

The feasibility study showed that substantial improvement could be reached by the introduction of some of the studied techniques. Accordingly, HSDPA specifications were published in Release 5 in March 2002, as shown in Figure 2.1. MIMO was not included in Release 5 specifications but later in Release 7 termed HSPA+ which is an enhanced version of HSPA [6]. Fast cell selection was discarded since it was concluded that the complexity introduced would not justify the benefits [1].

## 2.2. WCDMA principles

WCDMA is a Wideband Direct-Sequence Code Division Multiple Access (DS-CDMA), also known as direct-sequence spread spectrum. The following sections describe the technology of the 3rd generation of mobile communications, especially emphasizing the technology advantages and disadvantages.

### 2.2.1. Direct-Sequence Code Division Multiple Access

Code Division Multiple Access is a multi-channel access method. The main idea of this technology is to allow for sending independent information simultaneously over a single communication channel meaning that several users share common bandwidth.

Spread spectrum uses wide band, noise-like signals, see Figure 2.2. The user data signal is spread over a wide bandwidth by multiplying the user data with a code sequence of quasi-random symbols (called chips). Because spread spectrum signals are noise-like, they are hard to detect. Spread spectrum signals are also hard to intercept or demodulate. Further, spread spectrum signals are harder to jam than narrowband signals. These low probability of intercept and anti-jam features are why the military has used spread spectrum techniques for so many years. Spread signals are intentionally made to occupy a much larger bandwidth than the information they are carrying to make them look more noise-like.

Spread spectrum transmitters use similar transmit power levels than narrowband transmitters. However, they transmit at a much lower spectral power density than narrowband transmitters. Spread and narrow band signals can occupy the same band, with little or no interference. This capability is the main reason for all the interest in spread spectrum today [7].

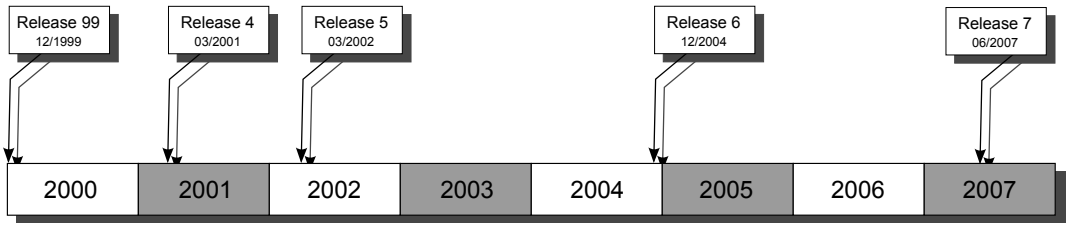


**Figure 2.1.:** 3GPP release timeline [1]

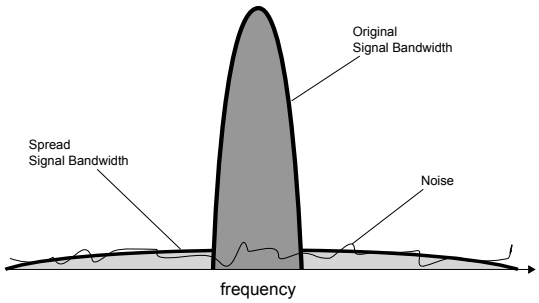


**Figure 2.2.:** Spread Spectrum

### DS-CDMA advantages and disadvantages

The use of DS-CDMA in cellular communications introduces several improvements and has certain advantages with respect to other multiple access schemes such as TDMA or FDMA. Let us briefly introduce some of them [7, 8]:

1. DS-CDMA systems imply a universal frequency reuse in each cell as all the cells use the entire available bandwidth. The frequency channel concept disappears making frequency planing much easier.

2. Narrowband interferences are now practically harmless. These interferences only affect certain parts of the spectrum. Because of the signal spreading, this narrowband interference will only have some impact to a small set of the signal (and thus, it affects only to a relatively small part of the overall power, as signal spreading implies also the spread of power along all the spectrum).

3. The lack of frequency channels enables User Equipments (UE) to be connected to more than one radio base station. Due to this, soft handovers can be done as well as macrodiversity techniques, which allows Radio Network Controllers (RNC) to combine different base station signals in order to make reception more robust.

4. Communication privacy is increased because only the transmitter and the receiver know the pseudo-noise sequence to despread the signal, and thus can decode the signal.

Nevertheless, CDMA systems have a certain number of disadvantages which are enumerated as follows:

1. Power requirements should be strictly controlled as DS-CDMA schemes are particularly sensitive to the Near-Far problem[1]. Despreading is more difficult when

[1] UEs may use the same carrier frequency and are distinguished only by the use of different spreading codes. In this case, the position of the users becomes relevant i.e. a UE closer to the base station

another station emits at a higher power. Due to this a power control system must be implemented [9].

2. Self jamming might appear. This effect happens when the supposed orthogonal coded sequences do not cancel each other perfectly due to multipath propagation.

3. A rigid chip-leveled synchronization is needed between transmitter and receiver.

### 2.2.2. Spreading and despreading

The spreading operation is the multiplication of each symbol of a data sequence of rate $R$ with a code sequence of $SF$ symbols, called chips. The result is a spreaded sequence of the data sequence at a rate of $SF \times R$. Spreading codes are chosen to be orthogonal among each other, i.e. the *inner product* between two codes is zero, see Appendix A.1. This wideband signal would then be transmitted across a wireless channel to the receiving end. The chip rate used in WCDMA is 3.84 Mcps leading to a carrier bandwidth of approximately 5 MHz.

At the receiver, the despreading consists of the multiplication of the spread data/chip sequence with the very same $SF$ code chip sequence that was used during the spreading of these symbols. Then the receiver integrates the resulting products for each user symbol. The increase of the data rate by $SF$ corresponds also to an increase of the spectrum occupied by a same factor. Despreading restores a bandwidth proportional to $R$ for the signal.

The Figure 2.3a depicts a spreading example when the chip sequence has length 5, and the transmitted user data sequence is modulated in BPSK and has a rate $R$. We see that the resulting sequence acquires the same appearance as the spreading code. During the despreading in the receiver, see Figure 2.3b, the original transmitted sequence can be recovered perfectly thanks to the orthogonality of the codes which have a cross-correlation equal to zero; in other words, they do not interfere with each other. Note that perfect synchronization is presumed [9].

### 2.2.3. Radio propagation

Air is the access medium for mobile communications. Also known as radio channel, this medium is highly hostile compared to the cabled transmission mediums.

may block a large part of the other users farther in the cell.

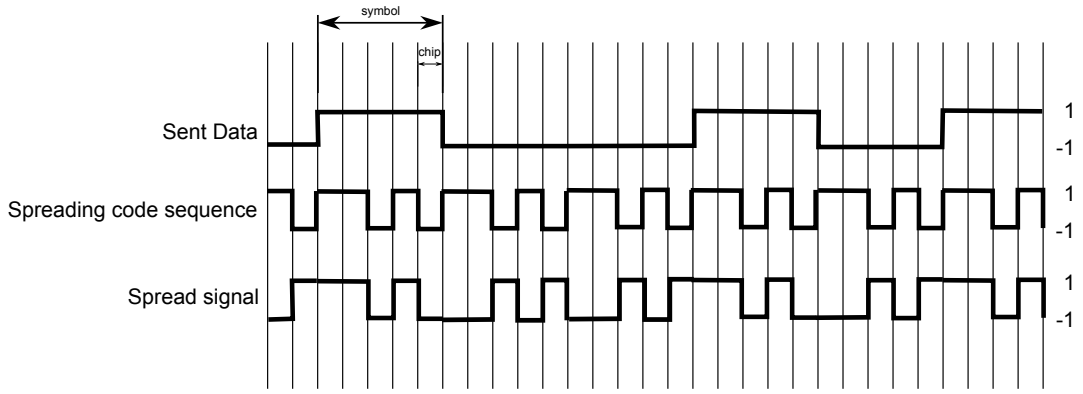


**(a)** Spreading

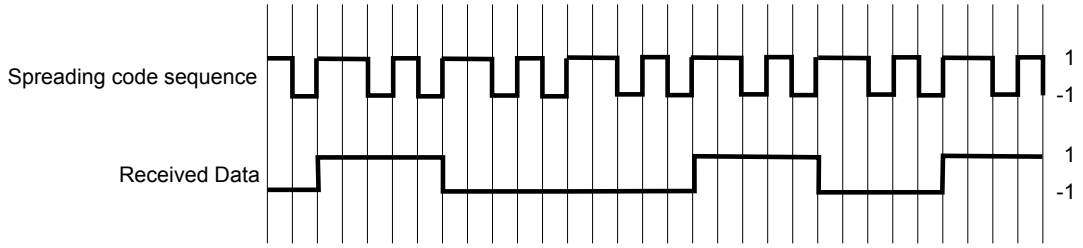


**(b)** A large subfigure

**Figure 2.3.:** Spreading and Despreading

Many propagations mechanisms are involved in radio channel transmissions that have effects on the signal. This section will deal with these mechanisms and its consequences. Besides, we will also focus on the propagation models that have been used in the present study.

### Propagation mechanisms in space with objects

As covered in the introduction of this section, radio channel transmissions suffer from a series of mechanisms that affect the signal quality. The main ones are reflection, diffraction and scattering [10].

- *Reflection* occurs when a propagating electromagnetic wave impinges on a smooth surface with very large dimensions compared to the signal wavelength ($\lambda$).
- *Diffraction* occurs when the radio path between the transmitter and receiver is obstructed by a dense body with large dimensions compared to ($\lambda$), causing secondary waves to be formed behind the obstructing body. Diffraction is a phenomenon that accounts for energy traveling from transmitter to receiver without a line-of-sight path between the two. It is often termed shadowing because the

diffracted field can reach the receiver even when shadowed by an impenetrable obstruction.

- *Scattering* occurs when a radio wave impinges on either a large rough surface or any surface whose dimensions are on the order of ($\lambda$) or less, causing the reflected energy t spread out (scatter) in all directions. In an urban environment, typical signal obstructions that yield scattering are lampposts, street signs and foliage.

These propagation mechanisms influence the signal propagation and cause different effects such as path loss, shadowing or multipath loss, which will be explained further on. These effects can be grouped as small-scale fading and large-scale fading [10].

### Small-scale fading

Small-scale fading affects the instantaneous signal power and therefore affects the link quality. There are fast and sudden changes on the signal power, which can vary 30 or 40 dBs in only a few seconds or within a few wavelength variations ($\lambda$). Fading can also create signal phase shifts (that is, changes in the signal space) and signal dispersion in time, known as echos. Fading is mainly caused by multipath propagation and by the Doppler effect which is caused by changing channel conditions (i.e. movement) [8, 7].

- *Multipath propagation.* Due to the reflection, diffraction and dispersion phenomenons, several signal versions are formed and arrive at the receiver with different phases, delays and amplitudes and as a result the signal suffers from large and fast power shifts. On the other hand, delays can cause symbol overlaps. This effect is known as Intersymbol Interference (ISI). The resulting signal can be represented as the sum of all the signal versions. So, for an emitted $x(t)$ signal, the received signal, formed from $N$ versions, will follow the next expression:

$$y(t) = \sum_{i}^{N} a_i(t,\tau)x(t-\tau_i(t))e^{j\phi_i(t,\tau)} \tag{2.1}$$

  where $a(t,\tau)$ is the signal attenuation, $\tau_i(t)$ represents the delay and $\phi_i(t,\tau)$ the phase difference.

- *Doppler effect.* This effect is produced when the wave-transmitter and its receiver are in relative movement. A change in phase is experienced with the consequent frequency shift, which is known as the Doppler frequency ($f_d$) and can be approximated to the following expression:

$$f_d = \frac{v}{\lambda} \tag{2.2}$$

where $\lambda$ is the wavelength and $v$ is the relative speed between transmitter and receiver. The degradation due to this effect can be split in two: *fast fading* and *slow fading*. When the coherence time of the channel (which is related with the Doppler frequency within a multiplicative constant) is short compared to the symbol duration, we say that the signal suffers from fast fading. In a fast fading situation, the channel is expected to change several times while a symbol is propagating causing a distorsion of the baseband pulse, resulting in a loss of signal-to-noise ratio (SNR) which may lead to an irreducible error rate. Slow fading occurs when the coherence time of the channel is long enough compared to the symbol duration. Then the channel is expected to remain unchanged during the time in which a symbol is transmitted [10].

### Large-scale fading

Large-scale fading affects the average signal power, mainly caused by free-space path loss and shadowing. It is well known that the power of an air-transmitted electromagnetic wave proportionally decreases with the squared distance to the transmitter. The received power expressed in terms of transmitted power is attenuated by a factor $L_s(d)$, where this factor is called free space loss. When the receiving antenna is isotropic this factor is expressed as:

$$L_s(d) = \left(\frac{4\pi d}{\lambda}\right)^2 \tag{2.3}$$

This effect is used in cellular systems because the rapid attenuation with distance makes it feasible to reuse channels and thus, increase system capacity. Not only free space propagation is affected by path loss, other parameters such as the base station or mobile antenna height or terrain characteristics are influencing too. The shadowing concept involves all the unique characteristics of the scenario which can hamper the communications and include for instance buildings and mountains. These environmental peculiarities increase the complexity of building up theoretical models [7, 8]. The following section presents the model used in the present study termed COST231 Walfish-Ikegami model which does not cover shadowing modeling.

### COST231 Walfish-Ikegami model

This empirical model is a combination of the models from J. Walfisch and F. Ikegami. It was further developed by the COST 231 project. It is now called Empirical COST-Walfisch-Ikegami Model.

The model considers the buildings in the vertical plane between the transmitter and the receiver. The accuracy of this empirical model is quite high because in urban

environments especially the propagation over the rooftops (multiple diffractions) is the most dominant part.

The main parameters of the model are listed in Table 2.1. Only the main equations are explain below, please refer to [11] for further details.

The model distinguishes between line-of-sight (LOS) and non-line-of-sight (NLOS) situations. In the LOS case, between base and mobile antennas within a street canyon, a simple propagation loss formula different from free space loss is applied. The loss is based on measurements performed in the city of Stockholm

$$L_b(\mathrm{dB}) = 42.6 + 25\log(d\,\mathrm{km}) + 20\log(f\,\mathrm{MHz}) \quad \text{for } d \geq 20\,\mathrm{m}. \tag{2.4}$$

In the NLOS-case the basic transmission loss is composed of the terms free space loss $\mathrm{L}_0$, multiple screen diffraction loss $\mathrm{L}_{\mathrm{msd}}$, and roof-top-to-street diffraction and scatter loss $\mathrm{L}_{\mathrm{rts}}$.

$$L_b = \begin{cases} \mathrm{L}_0 + \mathrm{L}_{\mathrm{rts}} + \mathrm{L}_{\mathrm{msd}} & \text{for } \mathrm{L}_{\mathrm{rts}} + \mathrm{L}_{\mathrm{msd}} > 0 \\ \mathrm{L}_0 & \text{for } \mathrm{L}_{\mathrm{rts}} + \mathrm{L}_{\mathrm{msd}} \leq 0 \end{cases} \tag{2.5}$$

The free-space loss is given by

$$\mathrm{L}_0(\mathrm{dB}) = 32.4 + 20\log(d\,\mathrm{km}) + 20\log(f\,\mathrm{MHz}). \tag{2.6}$$

The term $\mathrm{L}_{\mathrm{rts}}$ describes the coupling of the wave propagating along the multiple-screen path into the street where the mobile station is located. The determination of $\mathrm{L}_{\mathrm{rts}}$ is mainly based on Ikegami's model. It takes into account the width of the street and its orientation. COST 231, however, has applied another street-orientation function than Ikegami.

$$\mathrm{L}_{\mathrm{rts}} = -16.9 - 10\log(w\,\mathrm{m}) + 10\log(f\,\mathrm{MHz}) + 20\log(\Delta h_{\mathrm{Mobile}}\,\mathrm{m}) + L_{\mathrm{Ori}}. \tag{2.7}$$

Scalar electromagnetic formulation of multi-screen diffraction results in an integral for which Walfisch and Bertoni published an approximate solution in the case of base station antenna located above the roof-tops. This model is extended by COST 231 for base station antenna heights below the roof-top levels using an empirical function based on measurements. The heights of buildings and their spatial separations along the direct radio path are modelled by absorbing screens for the determination of $\mathrm{L}_{\mathrm{msd}}$.

$$\mathrm{L}_{\mathrm{msd}} = \mathrm{L}_{\mathrm{bsh}} + k_a + k_d\log(d\,\mathrm{km}) + k_f\log(f\,\mathrm{MHz}) - 9\log(b\,\mathrm{m}) \tag{2.8}$$

| *Parameters* | *Restrictions* |
|---|---|
| Frequency $f$ | 800 - 2000 MHz |
| Height of the transmitter $h_{TX}$ | 4 - 50 m |
| Height of the receiver $h_{RX}$ | 1 - 3 m |
| Distance $d$ between transmitter and receiver | 0.02 - 5 km |

**Table 2.1.:** Parameters COST231 Walfish-Ikegami model

## 2.3. HSDPA principles

This section covers HSDPA principles for WCDMA - the key new features included in Release 5, 6 and 7 specifications that are relevant for this study. HSDPA has been designed to increase downlink packet data throughput of release 99 by means of fast physical layer retransmission and transmission combining as fast link adaptation controlled by the base station. First a comparison between Release 99 and HSDPA is performed and then HSDPA key aspects are presented.

### 2.3.1. HSDPA vs Release 99 DCH

Three different methods for data packet transmission are specified in Release 99: Forward Access CHannel (FACH), Dedicated CHannel (DCH) and Downlink Shared CHannel (DSCH). The last one has been replaced in Release 5 for the new High-Speed Downlink Shared CHannel (HS-DSCH) and therefore will not be analyzed in this section. Table 2.2 shows the main differences between DCH and HS-DSCH channels, and it is explained in more detail below[1].

- *FACH.* This channel is used to transport small data volumes or connection set ups during state transfers. In HSDPA, it is used to carry signalling information when a terminal has changed its state. FACH does not support fast power control or soft handover. The Secondary Common Control Physical CHannel (S-CCPCH) is the responsible to carry its content and the used spreading code is fixed. If there is a need to carry mixed services, FACH cannot be used.
- *DCH.* The key part of Release 99 and Release 5 is always operated together with HSDPA. When circuit-switched service is demanded it runs always on DCH. In Release 5 the uplink user data always goes through the DCH, but in Release 6 there is an alternative with the use of an enhanced version of DCH (E-DCH). DCH can carry any kind of service using a fixed spreading code and fixed allocation time, although these parameters can be changed from upper layers. The theoretical maximum peak rate is 2 Mbps, in practice only 384 Kbps, and retransmissions are handled in the RNC. It supports the use of soft handover,

| *Feature* | *DCH* | *HS-DSCH* |
|---|---|---|
| Variable spreading factor | Yes | No |
| Fast power control | Yes | No |
| Adaptive modulation and coding | No | Yes |
| Multi-code operation | Yes | Yes, extended |
| Physical layer retransmissions | No | Yes |
| BTS-based scheduling and link adaptation | No | Yes |

**Table 2.2.:** Comparison DCH and HS-DSCH [1]

meaning that an UE can be connected with more than one station at a time and receiving information from all of them. The DCH also allows the use of the fast power control feature.

### 2.3.2. High-speed downlink shared channel

The logical transport channel, which carries the actual user data in HSDPA, is the HS-DSCH and is mapped physical channels named HS-PDSCH. The key differences between Release 99 DCH-based packet data operation, which are described in [1], are as follows:

- Lack of closed-loop power control or so called fast power control. In HSDPA, link adaptation selects the suitable combination of codes, coding rates, and modulation.
- Support of higher order modulation than DCH, the last release standardizes 64QAM, 16QAM and 4QAM for the downlink. In release 99 only 4QAM was available.
- The scheduling is done on a 2ms basis, with the addition of fast physical layer signaling. With DCH the Transmission Time Interval (TTI) could be as long as 80ms and not shorter than 10ms. The use of the new short allocation period implicitly implies a more dynamic nature of the system.
- Lack of soft handover. Data are sent from only one serving HS-DSCH cell.
- Lack of physical layer control information on the HS-PDSCH. This is carried on the High-speed shared control channel (HS-SCCH) for HSDPA use and on the associated DCH.
- Only spreading factor 16 is used, therefore the UEs will be able to support up to 15 codes because common channels and associated with DCHs need one of them. The support of multiple channelisation codes is called code-multiplex.

- Only turbo-coding is used, with DCH also convolutional code could be used.
- Implements Hybrid-ARQ (HARQ) which can operate in two modes: 'Chase combining' and 'incremental redundancy'.

### HS-DSCH coding

The use of turbo-coding outperforms convolutional codes, therefore HSDPA presents a restriction on the use of convolutional codes and just turbo-coding will be used from now on.

There are some changes introduced in the channel coding chain due to the use of new modulation schemes. Also a bit scrambling functionality is introduced to avoid having long sequences of '1s' or '0s', to ensure good signal properties for demodulation.

The HARQ functionality consists of two-stage rate matching functionality which allows tuning the redundancy version of different retransmissions when using non-identical retransmissions. HARQ can operate in two modes, 'Chase combining' or 'incremental redundancy' [1].

- In *Chase combining*, the rate matching is identical between transmissions so the same bit sequence is sent. The receiver stores the received samples as soft values, and therefore the memory consumption is higher than if it was storing hard values.
- *Incremental redundancy* uses a different rate matching between retransmissions. The relative number of parity bits to systematic bits varies between retransmissions. This solution requires more memory in the receiver. The rate matching function is varied between different retransmissions and in the actual implementation channel encoding can be done for each transmission or the data can then be kept in the virtual buffer.

When the physical retransmissions fail, these are handled by the RNC like in Release 99.

### HS-DSCH link adaptation

As covered in the section 2.3.2 the use of 2-ms TTIs allows the system a great dynamic. Apart from the scheduling decisions, the base station will also decide every 2 ms which coding and modulation combination to transmit.

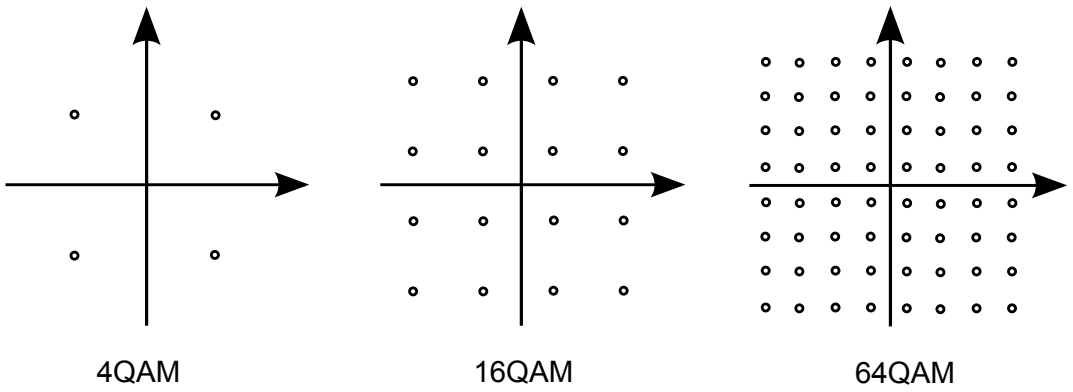


**Figure 2.4.:** Modulation constellations

Link adaptation is based on physical Channel Quality Indicator (CQI), which is the feedback provided by the UE. To avoid the near-far problem, link adaptation takes the extra power that results from being too close to the base station and uses it to select the transmission parameters in such way that the required symbol energy corresponds more accurately to the available symbol power. The dynamic range obtained using this technique can reach 30dB according to [1].

#### HS-DSCH modulation

The transport channel associated with R99, DCH, uses only 4QAM modulation. Release 5 and 6 offer additional support for higher modulation order on the downlink: 16QAM. Moreover Release 7, the so called HSPA+, introduces 64QAM on the downlink which increases the data rates by 50% and 16QAM on the uplink. The constellations are shown in Figure 2.4. The higher order modulation the higher the number of bits that can be carried per symbol. But higher order modulation introduces more complicated decision boundaries, and therefore the signal quality needs to be better when for example 16QAM is used instead of 4QAM. A good-quality CPICH allows the estimation of the optimum channel without user-specific pilot overhead [1, 12].

### 2.3.3. Multiple Input Multiple Output HSDPA

MIMO systems enable an increase of the throughput without having to increase the bandwidth nor the transmitted power. The same carrier frequency is used for all the transmitted antennas. These as well as the receiver antennas are usually uniformly separated by distances close to the size of a wavelength. MIMO HSDPA was introduced in Release 7 within what is called HSPA+ or HSPA evolved [6]. HSPA+

supports 2x2 downlink MIMO with up to two antennas at the transmitter and the receiver.

The standardized MIMO transmission scheme in Release 7 is termed Adaptative Antenna Array (see Figure 2.5). There are two modes defined: TxAA, in this case one stream is transmitted over both antennas, and D-TxAA or dual-stream TxAA, for this case, two separate data streams are transmitted on two orthogonal weight sets simulatneously. The weights $w_t^{(k)}$ are selected to maximize the signal-to-noise-and-interference ratio (SINR) at the UE. The weight selection is signaled by the UE to the base station. Note that when D-TxAA is used both data streams are transmitted on the same orthogonal spreading code(s). Thus, this achieves *code reuse*.

D-TxAA transmits the data streams using orthonormal array weight vectors drawn from the closed loop transmit diversity codebook. Because they are orthogonal, knowledge of one of the two array weight vectors will completely determine the other. In addition, it should be noted that in the MIMO case the second data stream is only turned on at high SINR conditions. In other words, either one data stream or two data streams are transmitted depending on the terminal SINR conditions.

MIMO performs most effectively when the SNR at the UE is high, ensuring a successful decoding of the signal in spite of distributing the power among the transmit antennas. MIMO also needs a rich scattering environment to keep the two data stream orthogonal when they reach the UE, so that there are enough uncorrelated paths, i.e. the channel matrix has to be of sufficient rank. Therefore MIMO benefits can be seen in dense urban areas where the size of the cells is typically small. Higher order modulation complements MIMO by providing significant gains in line-of-sight scenarios, where MIMO gains are limited.

The key benefits of MIMO systems compared to SISO systems summarized in [13] are:

- *Antenna grouping gain.* The processing in the transmitter and the receiver increases the mean SNR received.
- *Diversity gain.* The signal power in a wireless communication suffers from random fading. If the fading in each of the MIMO channels are uncorrelated, then better results will be obtained in detection. Thus, the more uncorrelated paths, the better the system will work. A diversity gain is obtained compared to SISO systems when there is just one path.
- *Spatial multiplexing gain.* MIMO channels provide an increase of the system capacity without the need to increase the bandwidth nor the transmitted power. This gain can also be enhanced by the capacity to transmit independent data signals in each of the transmission antennas.

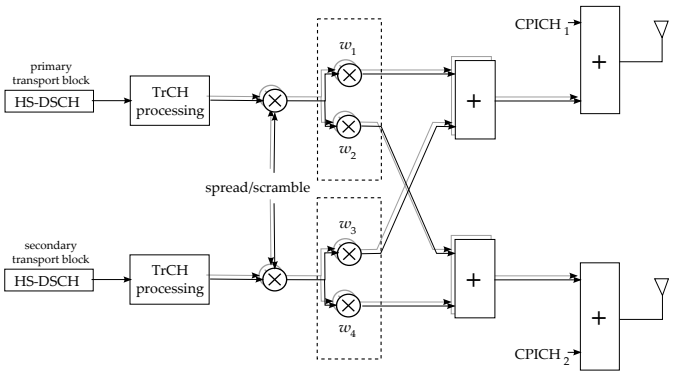


**Figure 2.5.:** Generic downlink transmitter structure MIMO D-TxAA [2]

### 2.3.4. HSDPA physical layer operation procedure

This section presents the HSDPA physical layer basic steps once at least one user have been configured to use HS-DSCH and the data is already present at the buffer of the base station [1].

- Every 2ms the base station evaluates each user in order to schedule which users will be served in the future. The selection criteria is not set in the standard, so schedulers are an ongoing research topic at the moment.
- When a UE is selected as served in a determined TTI, the base station identifies the HS-DSCH parameters needed for the transmission, including the number of codes, the modulation order and the UE limitations.
- HS-SCCH is transmitted two slots before the corresponding HS-DSCH TTI. This is because it has two different parts and Part 1 carries information needed to decode the frame HS-DSCH properly.
- The terminal monitors the HS-SCCHs (there are up to four). Once the Part 1 of HS-SCCH is decoded it will start to decode the Part 2 and will buffer the necessary codes from HS-DSCH.
- When decoding Part 2 the UE discovers the ARQ process, and can then determine whether there is the need of combining or not.
- After decoding, the UE sends in the uplink direction an ACK/NACK indicator after the combination of the data (if applied), depending on the result of the CRC over the HS-DSCH data.

# 3. Basic MIMO HSDPA Link-Level Simulator

This chapter presents the description of the implemented simulator used in this study to model a basic MIMO HSDPA link. The outline is as follows, Section 3.1 contains the general description of the simulation model. This is followed by a more detailed study of each component in Section 3.2. Finally, implementation issues are discussed in Section 3.3.

## 3.1. General structure

The general structure of our basic link level simulator is depicted in Figure 3.1. Basically, like in any communication system, there are three different parts: the transmitter, which in our case is the base station due to the study of the downlink (HSDPA); the channel, a MIMO frequency-selective channel plus Gaussian white noise; and finally the receiver or user terminal. All these elements are explained in detail in Section 3.2.

The *Basic MIMO HSDPA link-level simulator* emulates the physical transmission of the data channel (HS-DSCH) and the pilot channel (CPICH), the last one is used to estimate the channel for the data channel.

The bit sequences in the simulator flow encapsulated in packets of 2 ms, as cited before in Section 2.3.2 this is the TTI in HSDPA systems. For sake of simplicity and convenience the channel is constant during the duration of a TTI, i.e. block fading is utilized. The length of a radio frame is 10 ms and is composed of 15 slots, thus a TTI is formed by 3 slots.

## 3.2. Block Description

The dotted blocks in Figure 3.1 are presented in detail in Section 3.2.1, covering the generation of the CPICH and the HS-DSCH. In Section 3.2.2 we discuss the transmitter schemes supported in the simulator and introduce the concept of beamforming. The

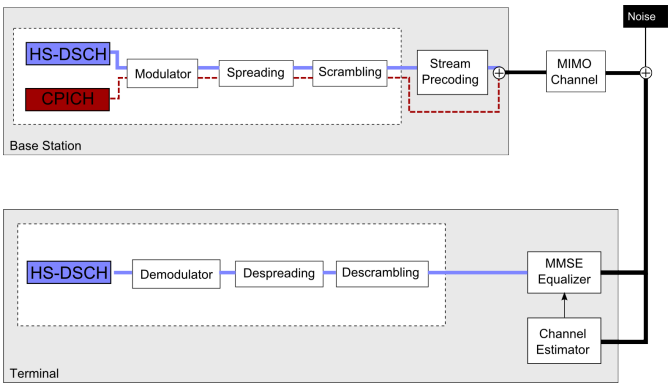


**Figure 3.1.:** Basic link-level simulator block diagram

channel model is covered in Section 3.2.3. This is followed by the receiver analysis in 3.2.4, emphasizing the new MMSE receiver preferred in HSDPA, as commented in [14]. Finally the schemes of channel estimators implemented in the simulator are discussed in Section 3.2.5.

### 3.2.1. Common Pilot Channel & High-speed Downlink Shared Channel

Before describing how the channels are created it is needed to understand the relation between the modulation, the spreading and the scrambling of the sequences. Figure 3.2 shows the relation between each other for a HS-DSCH stream taking into account that more than one bit stream is transmitted per stream. As can be seen, encoded rate-matched bits, $b_n^{(k)}[m]$, go through the modulation mapper in groups of the length according to the modulation selected. There are three modulation schemes supported in enhanced HSDPA [12]. Our simulation has support for all of them.

Once bits come out of the modulation mapper in shape of symbols, these are multiplied by the corresponding channelisation code, $C_{\mathrm{SF,c}}$, spreading the signal, and therefore increasing the symbol rate by the length of the channelisation code or spreading factor. In addition to spreading, part of the process in the transmitter is the scrambling operation. This is needed to separate UEs or base stations from each other. Scrambling is used on top of spreading, so it does not change the signal bandwidth but only makes the signals from different sources separable from each other [9]. The functionality and characteristics of the scrambling and channelisation codes for the HS-DSCH are summarised in Table 3.1. To understand how the channelisation and scrambling codes, $C_{scr}$, are generated, refer to Appendix A.1 and Appendix A.2, respectively.

| | *Channelisation code* | *Scrambling code* |
|---|---|---|
| Usage | Separation of connections to different users within one cell | Separation of sectors (cells) |
| Length | 16 chips | 2 ms = 7680 chips |
| Code family | Orthogonal Variable Spreading Factor | Long 10 ms code: Gold code Short code: Extended S(2) code family |
| Spreading | Yes, increases transmission bandwidth | No, does not affect transmission bandwidth |

**Table 3.1.:** Functionality of the channelisation and scrambling codes [9]

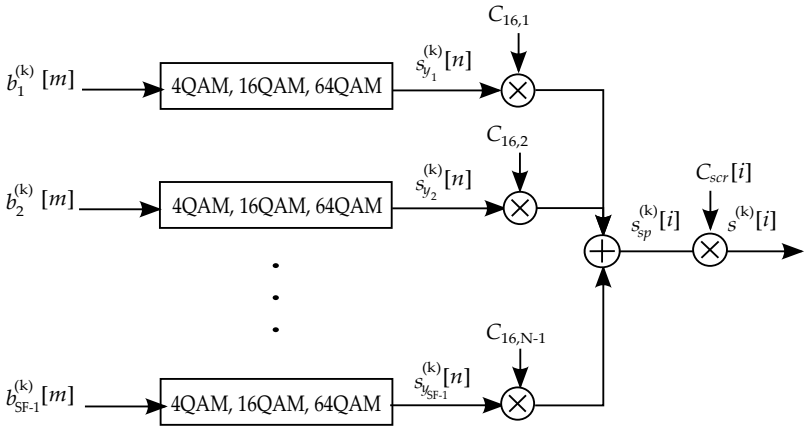


**Figure 3.2.:** Relationship between modulation, spreading and scrambling [3]

## CPICH

Figure 3.3 shows the structure of the CPICH as well as the bit sequence assigned to this channel. In case of MIMO transmission, the CPICH has to be transmitted from both antennas using the same spreading factor and scrambling code even though the pre-defined bit sequence of the CPICH is different for Antenna 1 and Antenna 2. When no diversity is used, Antenna 1 transmits just the sequence assigned to it.

Although there are two types of CPICH, only the primary (P-CPICH) is implemented in the simulator, the implementation of the secondary (S-CPICH)has no interest in this study. Normally each cell has only the P-CPICH, which is broadcasted to the entire cell. Occasionally the S-CPICH can be found implemented for serving dedicated hot-spot areas. This study focus on the optimization of the P-CPICH power, and therefore the term CPICH will be used for P-CPICH in the following.

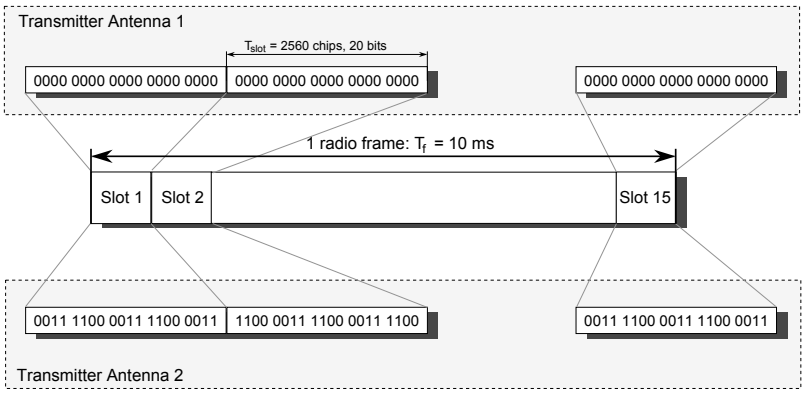


**Figure 3.3.:** Frame structure for Common Pilot Channel

The main features of the CPICH are the following [3]:

- The same channelisation code is always used and has length 256. Particularly the Orthogonal Variable Spreading Factor (OVSF)used is the $C_{256,0}$. (See Appendix A.1)
- The CPICH is scrambled by the primary scrambling code.
- The modulation scheme used is always 4QAM.
- There is only one CPICH per cell.
- CPICH is broadcast over the whole cell.
- The bit rate is 30 kbps, as a result of the use of spreading factor of 256, and 4QAM modulation it implies 20 bits per slot, and 2560 chips per slot. See Figure 3.3.

### HS-DSCH

For the data channel, the bit sequence is generated randomly with a length according to the spreading factor and modulation selected so that the number of chips transmitted during a TTI keeps constant. The equation (3.1) shows this relation

$$N_r = \frac{2560 \times M}{SF} \tag{3.1}$$

where $N_r$ denotes the number of bits to be generated, $M$ is the modulation order, $SF$ is the spreading factor used. Using the chip rate (3.84 Mcps) and the TTI (2 ms), the number of transmitted chips per TTI can be easily derived and the result is 7680 chips.

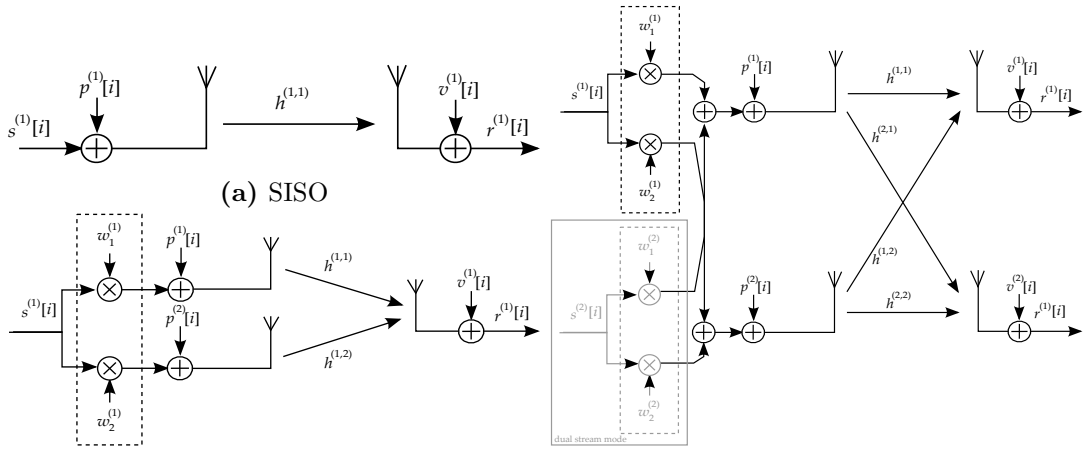


**Figure 3.4.:** Transmission schemes

A packet contains 3 slots, then the number of chips transmitted per TTI is equal to 2560 chips, here the origin of the constant.

The main characteristics of the HS-DSCH channel as implemented in the simulator are:

- The channelisation code has always length 16. There are 15 channelisation codes available from up to 16, one of them is reserved for the CPICH.
- The supported modulation schemes are 4QAM, 16QAM and 64QAM. The last one is standardized for the non MIMO case only.
- The bit rate is variable depending on the modulation.

### 3.2.2. Transmission modes

The simulator can cope with up to four different transmissions schemes (Figure 3.4): SISO, MISO 2x1, MIMO 2x2 TxAA, and MIMO 2x2 D-TxAA. Single-input single-output SISO(Figure 3.4a) and multiple-input and single-output MISO (Figure 3.4b) are degenerate cases of MIMO (Figure 3.4c), when respectively either only one transmitter and one receiver antenna or two transmitter and one receiver antenna are used. Release 7 includes the specification for the MIMO case limited to the two antenna scheme. Detailed information concerning MIMO HSDPA is presented in Section 2.3.3.

The standardized precoding vectors, which are used in multiple antenna cases, are defined as follows:

$$w_1^{(1)} = w_1^{(2)} = 1/\sqrt{2}$$

$$w_2^{(1)} = -w_2^{(2)}$$

$$w_2^{(1)} \in \left\{ \frac{1+j}{2}, \frac{1-j}{2}, \frac{-1+j}{2}, \frac{-1-j}{2} \right\}$$

Figure 3.4 also reflects the fact that no precoding is applied to the CPICH, denoted by $p^{(t)}$.

The spreading factor ($SF$) used for the data channel is $SF = 16$, one of them is reserved for CPICH. For this reason, each data stream has a capacity of 15 bit streams. Each bit stream is denoted in the Figure 3.2 as $b_n^{(k)}$ with $n \in 1...SF-1$ and $k$ is the stream index. Hence, as many as 30 different bit streams can be transmitted for a particular user, when D-TxAA is the selected mode.

The number of active streams in the case of our simulator is handled manually. Even though in general, a variable amount of power could be allocated to each stream in order to maximize capacity, this is not implemented in our simulator, because the extra complexity did not have substantial benefits for the purpose of this study, and therefore the power allocated to the data channel will be split equally among the number of streams.

### Selection of the best beamforming

The selection of the best beamforming is done according to [15]. The precoding matrix is selected in the transmitter in concordance with a past channel determined by a delay, $d_{bf}$. This is done because in a real system the best beamforming is selected in the UE and signaled to the base station which implies a certain delay.

The frequency-selective channel $\mathbf{H}_n$ is modeled as an array of length $L \times N_\mathrm{T}$ associated to the receiver antenna $n$. In order to maximize the received power, and therefore choose the best beamforming we define $\mathbf{R} := \sum_{n=1}^{N_\mathrm{R}} \mathbf{H}_n^\mathrm{H} \mathbf{H}_n$. Then the problem of choosing the weights $\mathbf{W}$, which is the matrix containing the precoding vectors, so that maximize the received power becomes

$$\underset{W:\|W\|^2=1}{\operatorname{argmax}} \ \mathbf{W}^\mathrm{H} \mathbf{R} \mathbf{W} \tag{3.2}$$

The optimal weight vector is the dominant eigenvector of $\mathbf{R}$. We always optimize over the first stream in the D-TxAA case.

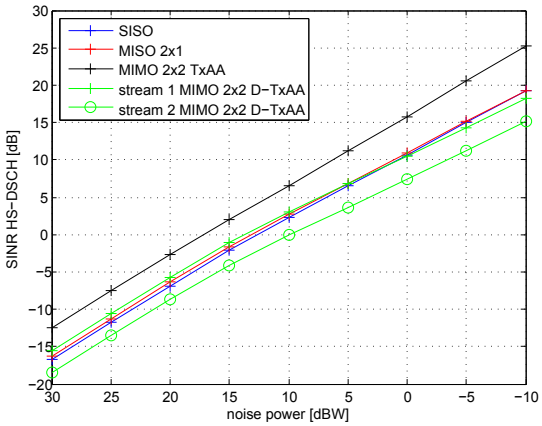


**Figure 3.5.:** Transmission scheme comparison

### Transmission schemes comparison

The HS-DSCH SINR is increased by the use of MIMO just as expected. This is depicted in Figure 3.5. The SINR in the case of MIMO D-TxAA is evaluated per stream. Note that in these simulations full knowledge of the channel is assumed in the equalizer.

The HS-DSCH SINR is the SINR observed at the demapper input, so after despreading and is obtained as follows: Consider the transmitted data symbol vector $\mathbf{s}_{y_n}^{(k)}$ of the $k$-th stream and $n$ spreading code (see Figure 3.2) and the corresponding received symbol vector at the demapper input $\hat{\mathbf{s}}_{y_n}^{(k)}$. The post equalization SINR then is given by

$$\mathrm{SINR}_{k,n} = \frac{\left\| \mathbf{s}_{y_n}^{(k)} \gamma^{(k)} \right\|_2^2}{\left\| \mathbf{s}_{y_n}^{(k)} \gamma^{(k)} - \hat{\mathbf{s}}_{y_n}^{(k)} \right\|_2^2} \tag{3.3}$$

where $\gamma^{(k)}$ represents the attenuation of the overall impulse response at delay $\tau$ and is given by

$$\gamma^{(k)} = \left\| \left( \mathbf{f}^{(\mathrm{k})} \right)^{\hat{\mathrm{H}}} \hat{\mathbf{H}}_w^{(\tau+(k-1)(L_f+L_h-1))} \right\|_2^2. \tag{3.4}$$

where $\mathbf{f}^{(\mathrm{k})}$ are the equalization filters for each $k$-th stream and $\hat{\mathbf{H}}_w^j$ denotes the column $j$ of the matrix $\hat{\mathbf{H}}_w$.

### 3.2.3. Channel model

The channel presents two types of fading effects: large-scale and small-scale fading, these effects have been presented in Section 2.2.3. In our simulator we deal with both of them. The interference power in the cell is modeled as a white Gausian noise and the channel is normalized to 1.

#### Small-scale fading

Small-scale fading are produced by changing channel conditions. The received signal is made up of multiple reflective rays, therefore the envelope amplitude due to small-scale fading has a Rayleigh probability density function [10] given by,

$$p(r) = \begin{cases} \frac{r}{\sigma^2} \exp\left[-\frac{r^2}{2\sigma^2}\right] & r \geq 0 \\ 0 & \text{otherwise} \end{cases} \tag{3.5}$$

where $r$ is the envelope amplitude of the received signal, and $2\sigma^2$ is the mean power of the multipath signal. Because of this sometimes the small-scale fading is also called *Rayleigh fading*. These interferences are generated as described in [16].

The channel will be fast fading or slow fading depending on the doppler frequency, $f_d$. As we have discussed before our simulator uses block fading, i.e. the channel is kept constant during the transmission of a packet (7680 chips or 2 ms). This limits our simulator so that the coherence time of the channel, $T_o$, must be larger than 2 ms. If the relative speed between the base station and the UE is $v = 3$km/h then $T_o \approx 32\ ms$ but when the speed turns to be $v = 50$ km/h then $T_o \approx 2\ ms$. This means that our simulator is limited to deal with relative speeds lower than 50 km/h. The attenuation introduced by the rayleigh fading for different velocities can be seen in 3.6.

In order to define the different number of propagation paths, we use the ITU channel model Pedestrian B [17], as specified in the standard [18]. Figure 3.7 shows the Power Delay Profile (PDP) of Pedestrian B model, which determines the length of the channel ($L_\mathrm{h}$). The maximum excess delay time, $T_m$, is also determined by the PDP. In this case, $T_m = 3700$ns. We can determine the duration of a chip, $T_c$, from the chip rate $R = 3.84$Mcps, which leads to a $T_c = 260.41$ns. Therefore the channel is frequency selective ($T_m > T_c$) and such multipath dispersion yields ISI. The equalization described in the next section mitigates these effects.

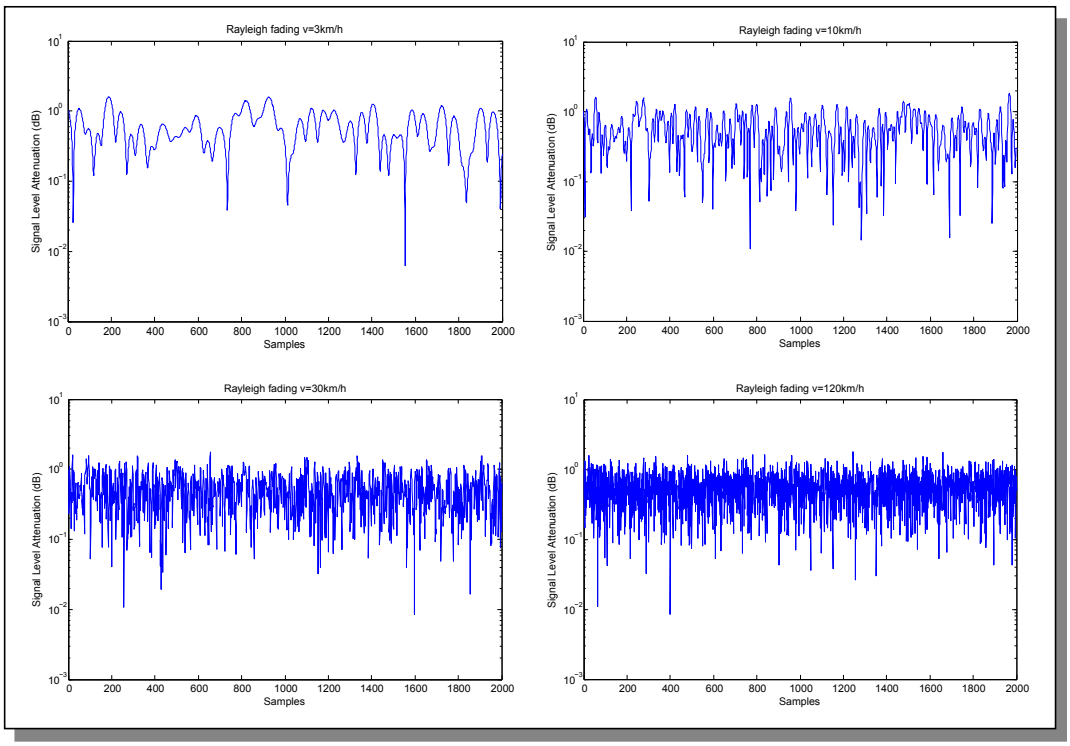


**Figure 3.6.:** Rayleigh fading for different speed

### 3.2.4. Equalization

RAKE is the conventional receiver for WCDMA which approximately implements a matched filter for the channel impulse response. The receive signal $r_i$ is first delayed and then descrambled, despread and combined to Maximum Ratio Combining (MRC), and the coefficients of the tap delay line are found through channel estimation.

HSDPA uses WCDMA for multiuser communication and thus orthogonal spreading codes are used to separate different users in the downlink. However, the orthogonality of these codes is destroyed by the multipath characteristics of the channel resulting in Multiple Access Interference (MAI). The performance of the MMSE equalizer is compared to the RAKE receiver in [14] proving that significant performance gain is obtained with the use of equalizers and that when these are used the overall system is no longer interference limited.

The MMSE equalizer implemented in our simulator is based on the papers [19, 20].

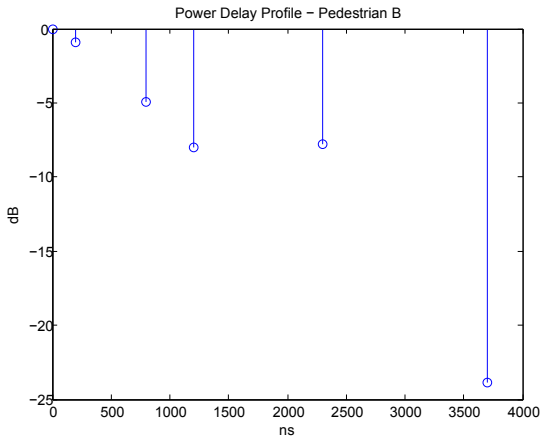


**Figure 3.7.:** PDP Pedestrian B

### System model

In order to derive an MMSE equalizer we present the system model as derived in [19]. The $k$-th spread and scrambled chip stream at time instant $i$ is defined as

$$\mathbf{s}_i^{(k)} = \left[ s^{(k)}[i], \ldots, s^{(k)}[i - L_\mathrm{h} - L_\mathrm{f} + 2] \right]^\mathrm{T}, \tag{3.6}$$

where $L_\mathrm{h}$ and $L_\mathrm{f}$ are the length of the channel impulse response and the equalizer length, respectively. The chip streams are weighted by the complex precoding coefficients $w_1^{(k)}$ and $w_2^{(k)}$ where the subindex indicates the transmit antenna. Afterwards the pilot sequences $p_i^{(1)}$ and $p_i^{(2)}$ are added at the resulting sequences in each antenna.

By stacking the transmitted stream vectors which can be up to $K = 2$, in case of D-TxAA and the CPICH vectors which depend on the number of transmit antennas,

$$\mathbf{s}_i = \left[ \left(\mathbf{s}_i^{(1)}\right)^\mathrm{T}, \ldots, \left(\mathbf{s}_i^{(K)}\right)^\mathrm{T} \right]^\mathrm{T}, \tag{3.7}$$

$$\mathbf{p}_i = \left[ \left(\mathbf{p}_i^{(1)}\right)^\mathrm{T}, \ldots, \left(\mathbf{p}_i^{(N_\mathrm{T})}\right)^\mathrm{T} \right]^\mathrm{T}. \tag{3.8}$$

The frequency selective channel between the $n_\mathrm{t}$-th transmit and the $n_\mathrm{r}$-th receive antenna is modeled by the $L_\mathrm{f} \times (L_\mathrm{h} + L_\mathrm{f} - 1)$ dimensional band matrix,

$$\mathbf{H}^{(n_r,n_t)} = \begin{bmatrix} h_0^{(n_r,n_t)} & \dots & h_{L_h-1}^{(n_r,n_t)} & 0 \\ \ddots & & \ddots & \\ 0 & h_0^{(n_r,n_t)} & \dots & h_{L_h-1}^{(n_r,n_t)} \end{bmatrix}, \tag{3.9}$$

where $h_i^{(n_r,n_t)}$ represent the channel impulse response of the $n_\mathrm{t}$-th transmit antenna to the $n_\mathrm{r}$-th receive antenna. Then, the full frequency selective MIMO channel is modeled by a block matrix $\mathbf{H}$ consisting of $N_\mathrm{R} \times N_\mathrm{T}$ band matrices defined in (3.9)

$$\mathbf{H} = \begin{bmatrix} \mathbf{H}^{(1,1)} & \mathbf{H}^{(1,N_\mathrm{T})} \\ \vdots & \vdots \\ \mathbf{H}^{(N_\mathrm{R},1)} & \mathbf{H}^{(N_\mathrm{R},N_\mathrm{T})} \end{bmatrix}. \tag{3.10}$$

By stacking the received signal vectors of all $N_\mathrm{R}$ receive antennas we have

$$\mathbf{r}_i = \left[ \left(\mathbf{r}_i^{(1)}\right)^\mathrm{T}, \dots, \left(\mathbf{r}_i^{(N_\mathrm{R})}\right) \right]^\mathrm{T}. \tag{3.11}$$

In addition to the channel effects a noise $\mathbf{v}_i$ term is added representing the thermal noise in the receiver and the interference power received from other base stations. This is modeled as an additive white gaussian noise (AWGN) with variance $\sigma_v^2$

We can obtain a compact system description of received symbols

$$\mathbf{r}_i = \mathbf{H}(\mathbf{W} \otimes \mathbf{I}_{L_\mathrm{h}+L_\mathrm{f}-1})\mathbf{s}_i + \mathbf{H}\mathbf{p}_i + \mathbf{v}_i = \mathbf{H}_w\mathbf{s}_i + \mathbf{H}\mathbf{p}_i + \mathbf{v}_i. \tag{3.12}$$

Here, $\otimes$ denotes the Kronecker product. The matrix $\mathbf{W}$ is defined in (3.13) containing the precoding values of each stream (up to K=2). How the selection of this precoding matrix is done is explained in Section 3.2.2.

$$\mathbf{W} = \begin{bmatrix} w_1^{(1)} & \dots & w_1^{(K)} \\ w_2^{(1)} & \dots & w_2^{(K)} \end{bmatrix} \tag{3.13}$$

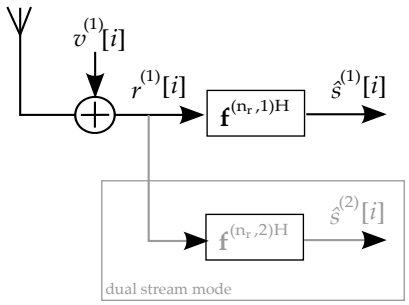


**Figure 3.8.:** MMSE equalizer structure

### ST-MMSE equalizer

The Space-time minimum mean square error (ST-MMSE) equalizer coefficients can be calculated by minimizing the distance between the equalizer chip stream and the transmitted chip stream through the following quadratic cost function [20]

$$J\left(\mathbf{f}^{(\mathrm{k})}\right) = \mathbb{E}\left\{\left|\left(\mathbf{f}^{(\mathrm{k})}\right)^{\mathrm{H}}\hat{\mathbf{r}}_i - s_{i-\tau}^{(1)}\right|^2\right\}, \tag{3.14}$$

where

$$\hat{\mathbf{r}}_i = \mathbf{H}_w\mathbf{s}_i + \mathbf{v}_i, \tag{3.15}$$

and

$$\mathbf{f}^{(\mathrm{k})} = \left[\left(\mathbf{f}^{(1,k)}\right)^{\mathrm{T}}, \ldots, \left(\mathbf{f}^{(N_{\mathrm{R}},k)}\right)^{\mathrm{T}}\right]^{\mathrm{T}}, \tag{3.16}$$

that defines $N_{\mathrm{R}}$ equalization filters for each $k$-th stream, see Figure 3.8. Each filter is defined by

$$\mathbf{f}^{(\mathrm{n_r,k})} = \left[f_0^{(n_{\mathrm{r}},k)}, \ldots, f_{L_{\mathrm{f}}-1}^{(n_{\mathrm{r}},k)}\right]^{\mathrm{T}}. \tag{3.17}$$

The minimization of the cost function is performed by deriving (3.14) with respect to $\left(\mathbf{f}^{(\mathrm{k})}\right)^*$ obtaining [20]:

$$\mathbf{f}^{(\mathrm{k})} = \sigma_s^2\left(\mathbf{H}_w\mathbf{R}_{ss}\mathbf{H}_w^{\mathrm{H}} + \mathbf{R}_{vv}\right)^{-1}\mathbf{H}_w\mathbf{e}_{\tau_k,2(L_{\mathrm{h}}+L_{\mathrm{f}}-1)}. \tag{3.18}$$

Here, the vector $\mathbf{e}_{\tau_k,2(L_{\mathrm{h}}+L_{\mathrm{f}}-1)}$ is a zero vector of length $2(L_{\mathrm{h}}+L_{\mathrm{f}}-1)$ with a single one at position

$$\tau_k = \tau + (k-1)(L_{\mathrm{h}}+L_{\mathrm{f}}-1) \quad k = 1\ldots K, \tag{3.19}$$

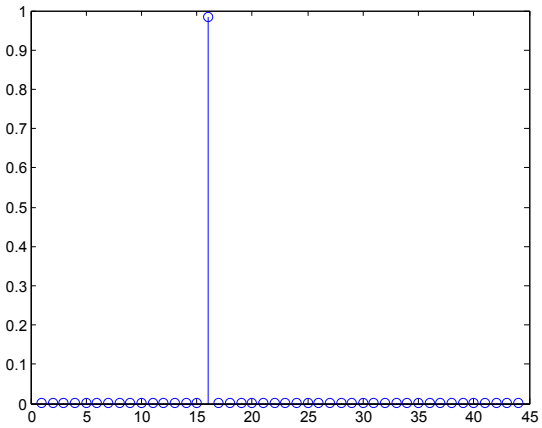


**Figure 3.9.:** Overall impulse response

The variable $\tau$ specifies the delay of the equalized signal and due to causality must fulfill the condition: $\tau \geq L_{\mathrm{h}}$. The matrices $\mathbf{R}_{ss}$ and $\mathbf{R}_{vv}$ are the signal and noise correlation matrices, respectively. Note that because we assume that the noise vector $v_i$ is AWGN with variance $\sigma_v^2$ and mean $\mu = 0$, the covariance matrix and the correlation matrix are the same and we can write $\mathbf{R}_{vv} = \sigma_v^2\mathbf{I}$. We also assume that the data signals of the users are uncorrelated and therefore $\mathbf{R}_{ss} = \sigma_s^2\mathbf{I}$ where $\sigma_s^2$ is the energy allocated to $k$-th stream.

Figure 3.9 shows an exemplary overall impulse response of the equalizer and channel, which is described in Section 3.2.3. It represents the ideal case when the noise term is assumed to be zero. The length of the impulse response is the sum of the length of the channel in this case is 18 chips because of the use of Pedestrian B, and the span of the equalizer which is 30 chips minus 1 chip, thus 47 chips.

### 3.2.5. Channel Estimation

Our simulator utilizes two channel estimators: Least Squares Estimator and the Correlation-based Estimator. Both of them are based on [21, 22].

#### System Model

In this case the spread pilot chip sequence $p_i^{(n_{\mathrm{t}})}$ and the spread data sequence $s_i^{(n_{\mathrm{k}})}$ are defined as follows

$$\mathbf{p}_{sp_i}^{(n_{\mathrm{t}})} = \left[p_{sp}^{(n_{\mathrm{t}})}[i] \ldots, p_{sp}^{(n_{\mathrm{t}})}[i + N_{\mathrm{c}} - 1]\right]^{\mathrm{T}}, \tag{3.20}$$

$$\mathbf{s}_{sp_i}^{(n_\mathrm{k})} = \left[ s_{sp}^{(n_\mathrm{k})}[i] \ldots, s_{sp}^{(n_\mathrm{k})}[i + N_\mathrm{c} - 1] \right]^\mathrm{T}, \tag{3.21}$$

where $i$ is the time index in chips and $N_\mathrm{c}$ is the number of chips considered for the channel estimation. In our case $N_\mathrm{c}$ will have the length of a packet, and therefore 7680 chips. The precoding of the data sequence is omitted by sake of simplicity and without lost of generality, note that the precoding could be done before the scrambling without alteration of the final transmitted sequence. Consequently, the scrambled transmit signal at antenna $n_\mathrm{t}$ is given by

$$\mathbf{x}_i^{(n_\mathrm{t})} = \mathbf{C}_{scr_i} \left( \mathbf{p}_{sp_i}^{(n_\mathrm{t})} + \mathbf{s}_{sp_i}^{(n_\mathrm{t})} \right) \quad n_\mathrm{t} = 1 \ldots N_\mathrm{T} \tag{3.22}$$

with the matrix $\mathbf{C}_{scr_i} = \mathrm{diag}[c_{scr_i}, \ldots, c_{scr_{i+N_\mathrm{c}-1}}]$ comprising the $N_\mathrm{c}$ chips of the base station's scrambling sequence at the main diagonal. The combined transmit signal for all $N_\mathrm{T}$ is modeled like this,

$$\mathbf{P}_{sp_i} = \left[ \mathbf{p}_{sp_i}^{(1)}, \ldots, \mathbf{p}_{sp_i}^{(N_\mathrm{T})} \right], \tag{3.23}$$

$$\mathbf{S}_{sp_i} = \left[ \mathbf{s}_{sp_i}^{(1)}, \ldots, \mathbf{s}_{sp_i}^{(N_\mathrm{T})} \right], \tag{3.24}$$

$$\mathbf{X}_i = \left[ \mathbf{x}_i^{(1)}, \ldots, \mathbf{x}_i^{(N_\mathrm{T})} \right] = \mathbf{C}_{scr_i} (\mathbf{P}_{sp_i} + \mathbf{S}_{sp_i}). \tag{3.25}$$

The definition of the channel in this section has been adapted according to [21]. The MIMO channel at the delay $k$ ($k = 0, \ldots, L_\mathrm{h} - 1$) is defined as

$$\mathbf{H}_k = \begin{bmatrix} h_k^{(1,1)} & \ldots & h_k^{(1,N_\mathrm{R})} \\ \vdots & \ddots & \vdots \\ h_k^{(N_\mathrm{T},1)} & \ldots & h_k^{(N_\mathrm{R},N_\mathrm{T})} \end{bmatrix} \tag{3.26}$$

we can define a stack matrix of the channel matrices like this

$$\mathbf{H} = \left[ \mathbf{H}_0^\mathrm{T} \ldots, \mathbf{H}_{L_\mathrm{h}-1}^\mathrm{T} \right]^\mathrm{T}. \tag{3.27}$$

Once we have defined our channel and the signal transmit in each antenna, we can express the receive signal of all receive antennas as

$$\mathbf{R}_i = \left[\mathbf{r}_i^{(1)}, \ldots, \mathbf{r}_i^{(N_\mathrm{R})}\right] = \sum_{k=0}^{L_\mathrm{h}-1} \mathbf{C}_{scr_{i-k}}(\mathbf{P}_{sp_{i-k}} + \mathbf{S}_{sp_{i-k}})\mathbf{H}_k + \mathbf{N}_i \tag{3.28}$$

The matrix $\mathbf{N}_i$ includes the interference of other base stations as well as the thermal noise at the receiver.

### Least Squares Estimator

Despite of being a low complexity channel estimator the Least Squares (LS) channel estimator has a reasonable good performance. From the model presented we can rewrite the equation (3.28) as

$$\mathbf{R}_i = \tilde{\mathbf{P}}_i\mathbf{H} + \tilde{\mathbf{N}}_i \tag{3.29}$$

where

$$\tilde{\mathbf{P}}_i = [\mathbf{C}_{scr_i}\mathbf{P}_{sp_i}, \mathbf{C}_{scr_{i-1}}\mathbf{P}_{sp_{i-1}}, \ldots, \mathbf{C}_{scr_{i-L_\mathrm{h}+1}}\mathbf{P}_{sp_{i-L_\mathrm{h}+1}}] \tag{3.30}$$

and

$$\tilde{\mathbf{N}}_i = \sum_{k=0}^{L_\mathrm{h}-1} \mathbf{C}_{scr_{i-k}}\mathbf{S}_{sp_{i-k}}\mathbf{H}_k + \mathbf{N}_i \tag{3.31}$$

Then, the LS estimator for the system description (3.29) is given by

$$\hat{\mathbf{H}}^{(\mathrm{LS})} = \left(\tilde{\mathbf{P}}_i^\mathrm{H}\tilde{\mathbf{P}}_i\right)^{-1}\tilde{\mathbf{P}}_i^\mathrm{H}\mathbf{R}_i \tag{3.32}$$

### Correlation-based Estimator

The correlator estimator is a simplified case of the LS estimator. It tries to avoid the calculation of the matrix $\left(\tilde{\mathbf{P}}_i^\mathrm{H}\tilde{\mathbf{P}}_i\right)^{-1}$. The approximation and therefore the correlation-based estimator is given by

$$\hat{\mathbf{H}}^{(\mathrm{cor})} = \frac{1}{\|\mathbf{p}\|_2^2}\tilde{\mathbf{P}}_i^\mathrm{H}\mathbf{R}_i \tag{3.33}$$

Where the term $\|\mathbf{p}\|_2^2$ denotes the energy of the CPICH sequence transmitted at one transmit antenna.

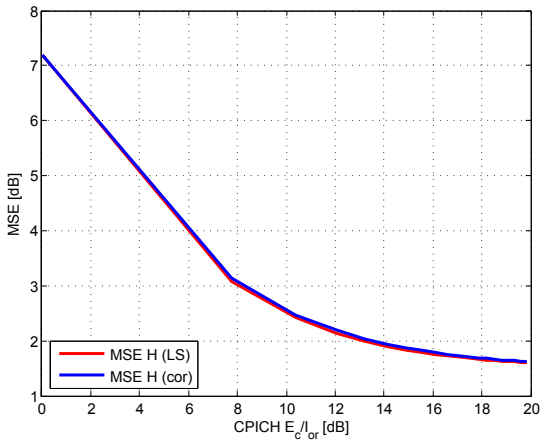


**Figure 3.10.:** Comparison of channel estimators

#### Comparison of channel estimators

Correlation-based estimator is a simplified version of the LS estimator, therefore a similar result is expected. The mean square error (MSE) of both channel estimators for a SISO case and a noise power of -4dBW is depicted in figure 3.10, they look very much the same over a large range of values, but it can also be observed that the larger the power allocated to the common pilot channel the larger the difference between the channel estimator MSE.

## 3.3. Implementation issues

The Basic MIMO HSDPA link-level simulator is implemented in MATLAB. The tools provided by MATLAB are very powerful and useful for the purpose of this study, because some of the functions such as convolution and filtering are already implemented.

The main file structure of the simulator is depicted in Figure 3.11 . The structure of the simulator is contained in hsdpa_link_body file. E_HSDPA_link level_simulator file contains the different simulations which has been used in this study, it offers the possibility of being upgraded with more simulations. Each simulation file simu_xxx has associated a load_parameters_xxx file, which has the parameters that can be set by the user for the chosen simulation.

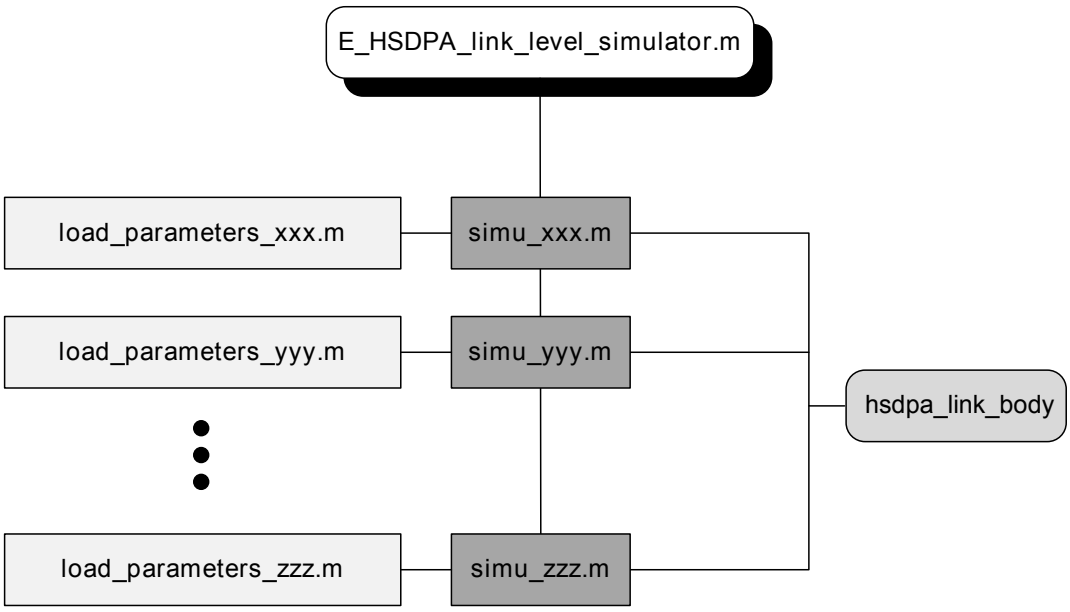


**Figure 3.11.:** Basic MIMO HSDPA link-level simulator file structure

# 4. Mobile Network Simulations

This chapter presents the importance of system-level simulators and computational efficient modeling. First, the differences between link-level and system-level simulators are covered in Section 4.1. In Section 4.2 we present a computationally efficient MIMO HSDPA system-level simulator showing its main structure and focusing in the link-measurement model. Finally in Section 4.3, we propose a model improvement to take into consideration the effects of channel estimation in the link-measurement model.

## 4.1. System-Level Simulations vs. Link-Level Simulations

*Link-level simulators* are commonly used to study the behavior of transmission and reception schemes. As the name indicates, this kind of simulators just study one link, in this case we are talking about the link between one UE and one base station. Link-level simulators aim to study the physical characteristics of the link and sometimes some MAC functionalities such as development of receiver algorithms, feedback strategies, coding design, and so on.

Mobile Network Operators (MNO) are aware that an optimization of their networks increases the performance and reduces costs. For this reason, it is important to identify whether, and to which amount, predicted link level performance gains can be obtained in an entire network. Hence, a comprehensive study of a mobile network technology can not stick just to the way how one UE performs with the base station. The goal of *system-level simulators* is to evaluate the performance of a whole network (or part of it), where multiple users, multiple cells and therefore base stations are taken into consideration. Cell planning, scheduling and multi-user and multi base station interference are some of the investigations that system-level simulators try to cover. This type of simulators have to rely on simplified link models that still must be accurate enough to capture the essential behavior due to complexity reasons because the computational cost of evaluating a whole network with the use of link-level simulators is prohibitive[23].

In this study the implemented basic MIMO HSDPA link-level simulator (see Chapter 3) is used to enhance the characteristics of the MIMO HSDPA system-level simulator in [23, 5].

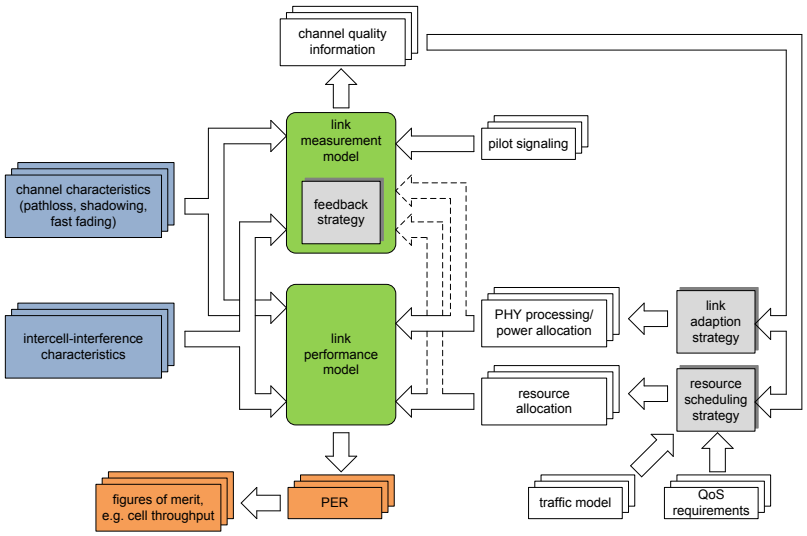


**Figure 4.1.:** Schematic block diagram of system level simulations [4]

## 4.2. MIMO HSDPA System Level Simulator

Figure 4.1 depicts a schematic diagram of a basic dynamic system-level simulator. Generally two kind of models are required: a link measurement model, which models the measurement used for link adaptation and resource allocation, and a link performance model, which determines the BLock Error Ratio (BLER) given a certain resource and power allocation as well as signal processing. Both models are related in the sense that they provide figures for performance prediction and can be referred to as *system level interface* [23]. The following sections present the main structure of the MIMO HSDPA System-level simulator and how these two models are implemented.

### 4.2.1. General Structure

In [5] a computationally efficient link-to-system level model is proposed and its embedding in a MATLAB-based system-level simulator which includes as features MIMO with D-TxAA, and a Minimum Mean Squared Error (MMSE) equalizer. This system-level simulator presented shows a structure that identifies the relevant interference terms and allows for the generation of scalar fading parameters prior to system-level simulation. Utilizing this special structure nearly all link-dedicated procedures can be included in these fading parameters, thus during the runtime of the system level simulation only scalar multiplications are needed to compute the SINR, thus reducing significantly the computational effort.

The structure of the simulator is depicted in Figure 4.2. It can be decomposed in the main network elements [23]:

- *Node B.* It represents all network related procedures, in particular it carries out the scheduling trying to balance the throughput and fairness as well as the Transport Format Combination (TFC) decision based the UE feedback.
- *SL model.* The channel model is represented using an abstract model, so that it needs lower computational complexity, even though it is capable of support different transmission schemes and receivers.
- *UE.* User specific algorithms and feedback decisions are done here. In addition, the evaluation of the transmission success is performed.
- *delay.* A signaling delay is imposed.

In following sections we will focus on the link-measurement model since the improvements in this study will be done on this model. Only a short reference to the link-performance model is done, but more information can be found in [23].

### 4.2.2. Link-Measurement Model

This model reflects base station and terminal measurements, such as estimated SINR used for channel dependent scheduling and link adaptation. Measurement results not only depend on channel and inter-cell interference, in fact, they also depend on the measurement phase as for example transmission power and beamforming weights. This model is needed to provide appropriate estimates of the channel quality.

In this section we present the system model utilized in [23] to derive the computationally efficient link-measurement model, we explain shortly the main parts and let the reader refer to [23] for finding more detailed information.

#### System model

Figure 4.3 depicts the model where the transmitter (Tx) and the receiver (Rx) are equipped with $n_{\mathrm{T}}$ and $n_{\mathrm{R}}$ antennas, respectively. Accordingly the input data stream $\mathbf{s}$ is demultiplexed into $N$ parallel streams, $s_0, \ldots, s_{N-1}$ with the individual data streams $s_n$, $0 \leq n \leq N-1$, being spread by a number of spreading sequences, $\varphi_n$ (multi-code usage) and scrambling sequences.

These spread and scrambled sequences are then mapped to the $n_{\mathrm{T}}$ transmit antennas using a prefiltering matrix $\mathbf{D} \in \mathbb{C}^{n_{\mathrm{T}} \times N}$, which contains the precoding weights, $w_1, \ldots, w_{n_{\mathrm{T}}N}$. In this work the maximal amount of streams and transmitter antennas is fixed to 2, and therefore there will be 4 precoding weights. At the receiver, the

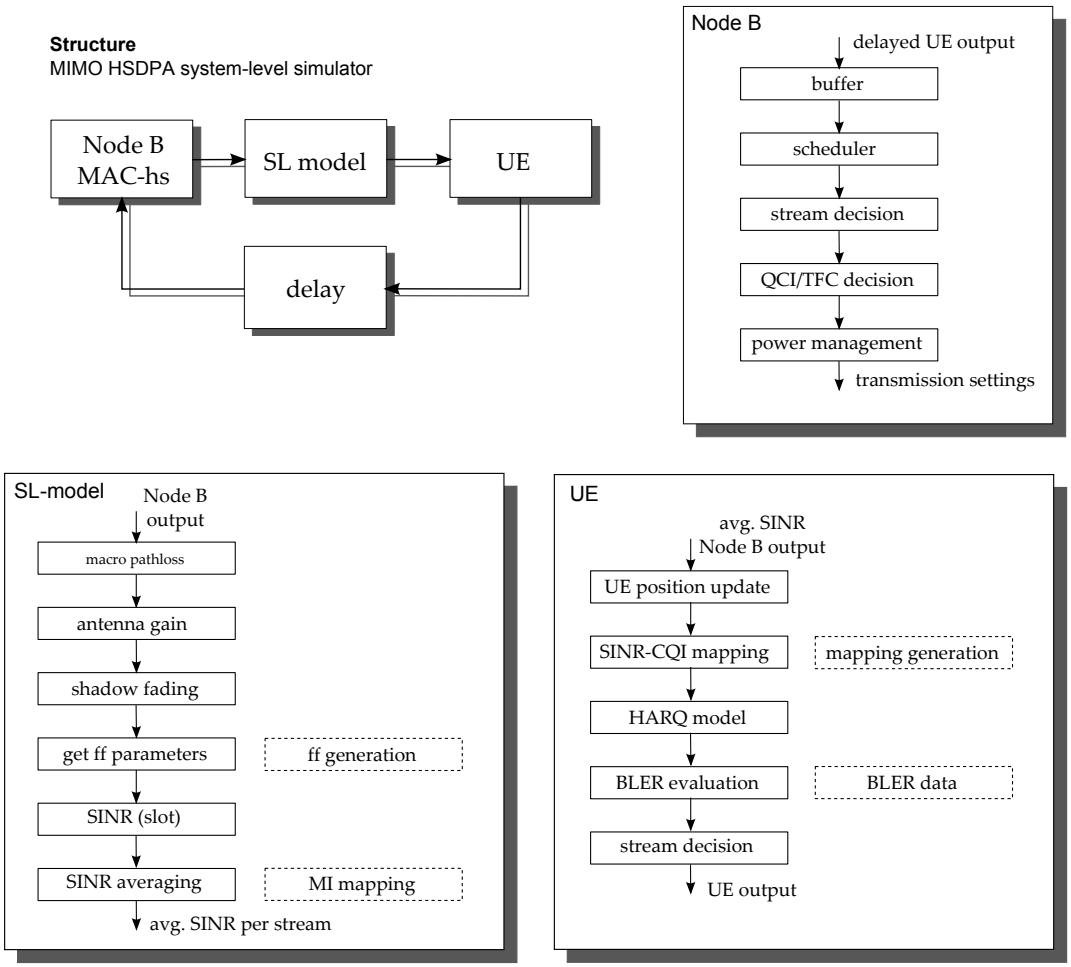


**Figure 4.2.:** MIMO HSDPA system-level simulator main structure

signals are gathered with $n_{\mathrm{R}}$ antennas and chip spaced sampled before they enter the discrete time ST-MMSE equalizer. The MIMO channel $\mathbf{H} \in \mathbb{C}^{n_{\mathrm{R}} \times n_{\mathrm{T}} L}$ is modeled as time-discrete, frequency-selective channel,

$$\mathbf{H} = \begin{bmatrix} h_{1,1}(0) & \dots & h_{1,n_{\mathrm{T}}}(0) & \dots & h_{1,n_{\mathrm{T}}}(L-1) \\ \vdots & \vdots & \vdots & \ddots & \vdots \\ h_{n_{\mathrm{R}},1}(0) & \dots & h_{n_{\mathrm{R}},n_{\mathrm{T}}}(0) & \dots & h_{n_{\mathrm{R}},n_{\mathrm{T}}}(L-1) \end{bmatrix} \tag{4.1}$$

where the entry $h_{r,t}(l)$ denotes the l-th sampled chip of the channel impulse response from transmit antenna $t$ to receive antenna $r$, with a total length of $L$ chip intervals. Note that the pulse shaping the transmit and receive filtering, as well as the sampling

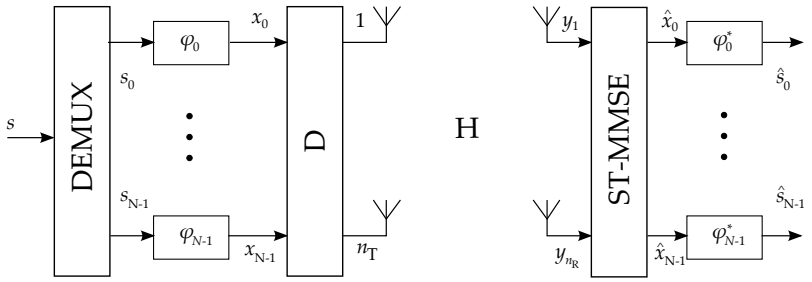


**Figure 4.3.:** System Model

operation can be incorporated in the MIMO channel matrix. For sake of notational simplicity, an equivalent discrete channel $\Gamma \in \mathbb{C}^{n_R \times n_T L}$ is defined that includes the prefiltering matrix $\mathbf{D}$ and the MIMO channel $\mathbf{H}$, i.e. $\mathbf{\Gamma} = \mathbf{H} \cdot (\mathbf{I}_L \otimes \mathbf{D})$, with $\mathbf{I}_L$ denoting the identity matrix of size $L$, and $\otimes$ being the Kronocker product. With this, the input output relation at time instant $k$, formulated by means of the equivalent channel matrix, is given by

$$\mathbf{y}(k) = \mathbf{\Gamma}\mathbf{x}(k) + \mathbf{n}(k), \tag{4.2}$$

where we introduced the receive vector $\mathbf{y}(k) = [y_1(k), \ldots, y_{n_R}(k)]^T$, the transmit vector $\mathbf{x}(k) = [x_0(k), \ldots, x_{N-1}(k), \ldots, x_{N-1}(k-L+1)]^T$ and the receive noise vector $\mathbf{n}(k) = [n_1(k), \ldots, n_{n_R}(k)]^T$.

The ST-MMSE solution can be computed again according to Equation (3.14).

### Equivalent Fading Parameteres Description

In this section we just present the conclusions obtained in [23]. The receive power is decomposed into different interference terms to derive the system level model. With this decomposition it is possible to describe the characteristics of the individual terms by means of fading-parameters that are real valued scalar processes. These parameters can be computed offline and loaded for the runtime of a system-level simulation, thus significantly reducing the computational burden.

First of all we decomposed the equalizer coefficients $\mathbf{W}_d = [\mathbf{w}_1, \ldots, \mathbf{w}_n, \ldots, \mathbf{w}_N]^T$ and the channel $\Gamma_{u,b} = [\gamma_{u,b}^0, \ldots, \gamma_{u,b}^m, \ldots, \gamma_{u,b}^{N(E+L-1)-1}]$ where $n$ denotes the stream index and m is the index of the Tx chips for all streams entering the equalizer span. Without losing generality, the user $u = 0$ and the base-station $b = 0$ are the one defined of interest.

1. *Desired Signal:* The desired power signal is given by

$$P_{s,n} = \left| \mathbf{w}_n^T \gamma_{00}^{dN+n} \right|^2 \cdot P_{n,\zeta} = G_{s,n} \cdot P_{n,\zeta} \tag{4.3}$$

where $P_{n,\zeta}$ denotes the power on stream $n$ and spreading code $\zeta$ spent for user $u = 0$ by base-station $b = 0$. $G_{s,n}$ describes the equivalent fading of the useful signal power.

2. *Intracell Interference:* The intracell interference is composed by a number of terms, i.e. the remaining ISI after equalization, the intercode interference when the same scrambling but a different spreading code is used, the intracell interference from users that are not served in the same instant as the user of interest but with the same instant as the user of interest but with the same scrambling and spreading code, and the intracell interference from users with the same scrambling but different spreading code. The following equation represents a simplification of all this interferences.

$$P_{intra,n} = \left[ P_0 + o_{\mathrm{BF},n} \cdot \sum_{u=1}^{U_0} P_u \right] \cdot o_{intra,n} \cdot G_{s,n}, \tag{4.4}$$

where the intra-cell orthogonality, $o_{intra,n}$, is defined as

$$o_{intra,n} \triangleq \frac{1}{N} \cdot \frac{\sum_{\substack{m=0 \\ m \notin [dN, dN+N-1]}}^{N(E+L-1)-1} \left| \mathbf{w}_n^T \gamma_{00}^m \right|^2}{\left| \mathbf{w}_n^T \gamma_{00}^{dN+n} \right|^2}, \tag{4.5}$$

and the pre-coding orthogonality, $o_{\mathrm{BF},n}$, is given by

$$o_{\mathrm{BF},n} \triangleq \frac{1}{G_{s,n}} \frac{1}{|\Omega|} \sum_{\omega \in \Omega} \sum_{\substack{m=0 \\ m \notin [dN, dN+N-1]}}^{N(E+L-1)-1} \left| \mathbf{w}_n^T \gamma_{\omega 0}^m \right|^2 \tag{4.6}$$

3. *Intrastream Interference:* The interference generated by the parallel transmission of a second stream is given by

$$P_{\mathrm{INT},n} = \sum_{\substack{m=0 \\ m \neq n}}^{N-1} \left| \mathbf{w}_n^T \gamma_{00}^{dN+m} \right|^2 \cdot P_{m,\zeta} = G_{s,n} \cdot \sum_{\substack{m=0 \\ m \neq n}}^{N-1} o_{\mathrm{INT},m} \cdot P_{m,\zeta}, \tag{4.7}$$

where $o_{\mathrm{INT},n} \triangleq \left| \mathbf{w}_n^T \gamma_{00}^{dN+m} \right|^2$ denotes the intrastream orthogonality factor.

4. *Intercell Interference:* This interference term assumes that all users in a neighbouring cell will apply the same pre-coding coefficient, and that all substreams designated for one user are equally powered. Having considered this the intercell interference is given by

$$P_{inter,n} = \sum_{b=1}^{B} P_{\mathrm{tot},b} \frac{1}{N} \mathbf{w}_n^{\mathrm{T}} \left[ \sum_{m=0}^{N(E+L-1)-1} \gamma_{0b}^m (\gamma_{0b}^m)^{\mathrm{H}} \right] \mathbf{w}_n^* = \sum_{b=1}^{B} P_{\mathrm{tot,b}} G_{\mathrm{inter},b,n}, \tag{4.8}$$

5. *Thermal Noise:* The thermal noise is modeled as i.i.d. white Gaussian noise, with identical power on all antenna and over all chips that enter the equalizer. The power (on symbol level) of the thermal noise can denoted as

$$W = \mathbb{E}\left\{\left\|\mathbf{w}_n^{\mathrm{T}}\mathbf{n}_E(k)\right\|_2^2\right\} = \sigma_{\mathbf{n}}^2\left\|\mathbf{w}_n^{\mathrm{T}}\right\|_2^2. \tag{4.9}$$

#### Influence of Non-Data Channels

The intereference caused by non-spread channels is given by

$$P_{\mathrm{ns},n} = \frac{P_{\mathrm{non-spread}}}{N} G_{s,n}\left[1 + \sum_{\substack{m=0 \\ m\neq n}}^{N-1} o_{\mathrm{INT},m}\right] + P_{\mathrm{non-spread}} o_{\mathrm{intra}} G_{s,n} \tag{4.10}$$

and the interference caused by other spread channels than HS-DSCH assuming the total power of other spread channels in the cell to be $P_{\mathrm{other-spread}}$, can be evaluated to be

$$P_{\mathrm{s},n} = P_{\mathrm{other-spread}} o_{\mathrm{intra,n}} G_{s,n} \tag{4.11}$$

#### Resulting SINR Description

The SINR on substream $n$ and spreading code $\zeta$, as observed after equalization and despreading, taking into consideration all the exposed above, can be expressed by

$$\mathbf{SINR}_{n,\zeta} = \frac{\mathrm{SF}\cdot P_{s,n}}{\mathrm{SF}\cdot P_{\mathrm{INT},n} + P_{\mathrm{intra},n} + P_{\mathrm{ns},n} + P_{\mathrm{s},n} + P_{\mathrm{inter},n} + W}, \tag{4.12}$$

where SF denotes the spreading factor and $P_{\mathrm{INT},n}$ simplifies to $P_{\mathrm{INT}} = o_{\mathrm{INT}} \cdot G_{s,n} \cdot P_{m,\zeta}$ for the case D-TxAA, since there is only one interfering parallel substream.

### 4.2.3. Link-Performance Model

The link performance model provides an estimate of the link performance when the decisions on the radio resource management (RRM), scheduling and link adaptation are already known. This model generates either a bit or a block error probabilities and is utilized for quality estimation at run-time, which in turn can generate, for example retransmissions and affect also slow link adaption. Such a model can be viewed as a conditional probability; the probability that the transmitted code word is decoded erroneously given the channel, Tx power, beamforming weights and interference plus noise during the interleaving period [24].

| Parameter | Value |
|---|---|
| power allocated at HS-DSCH | 20 W |
| channel model | ITU PedB |
| equalizer length $L_f$ | 30 chips |
| equalizer delay $\tau$ | 15 chips |
| number of spreading factors per stream | 15 |
| channel estimator | full knowledge of the channel |

**Table 4.1.:** SINR validation simulation settings

## 4.3. Link-measurement model enhancement

This section presents a validation of the current link-measurement model, and shows the fact that there is the effect of the channel estimation missing, and therefore its link with the power assigned to the common pilot channel. An improvement of the current model is presented, which extends the capabilities of the MIMO HSDPA system-level simulator.

### 4.3.1. Validation of the current model

In order to validate the link-measurement model presented in [23], an adaptation of the model has been implemented in the basic MIMO HSDPA link-level simulator presented in Chapter 3. The intercell interference and the interference due to the influence of non-data channels has been omitted since they are not implemented in the basic link-level simulator.

Figure 4.4 depicts the performed simulations to validate the proposed SINR description, for each transmission scheme. The *genie* SINR is the SINR observed at the demapper input, so after de despreading and is obtained as defined in (3.3).

The main simulation parameters can be seen in Table 4.1. Notice that full knowledge of the channel is assumed. It can be observed that the link-measurement model shows a very good agreement with the *genie* or *true* SINR.

### 4.3.2. Influence of CPICH in the current model

The CPICH is a very important channel since the channel estimation in the UE is performed according to this. Figure 4.5a depicts the MSE of the channel coefficients, defined as

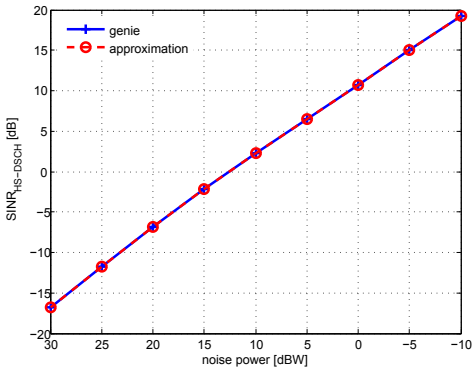


**(d)** SISO

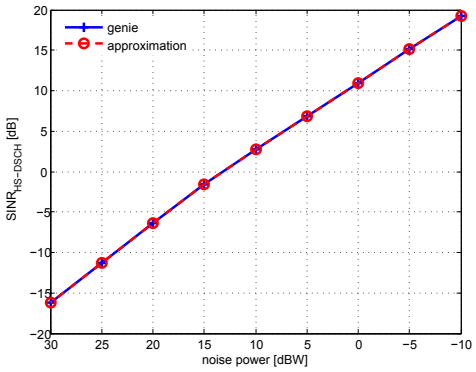


**(e)** MISO 2x1

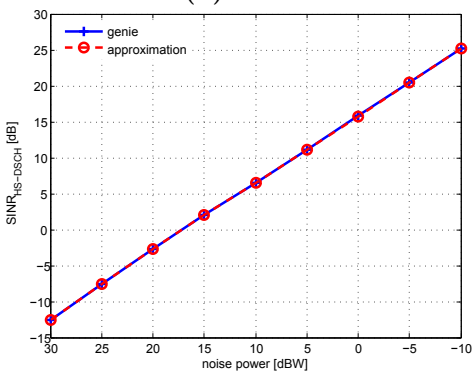


**(f)** MIMO 2x2 TxAA

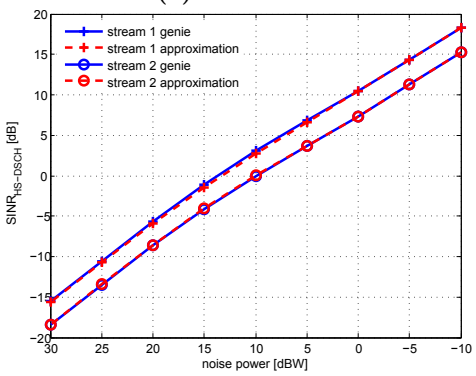


**(g)** MIMO 2x2 D-TxAA

**Figure 4.4.:** Model validation

$$\mathrm{MSE}(\hat{h}) = \mathbb{E}\left\{\left\|\hat{h} - h\right\|^2\right\} \tag{4.13}$$

where $\hat{h}$ are the estimated channel coefficients using the LS estimator or the correlation-based estimator. The result is obvious, a smaller MSE is obtained when the power allocated to the CPICH is higher. It is also important to notice that the curves are unique for a certain CPICH SINR or CPICH$_{E_c/I_0}$. Figures 4.5b-4.5d, show the MSE for the rest of schemes, note that the MSE increases with the channel complexity.

The link-measurement model, described in Section 4.2.2, does not take into account this effect and supposes a perfect knowledge of the channel when performs the equalization, which is a situation far from the reality. The consequence is a poor performance of the approximation when the CPICH is considered. Figure 4.6 depicts the effect, where in each case, the lower curve denotes a dependence with the MSE

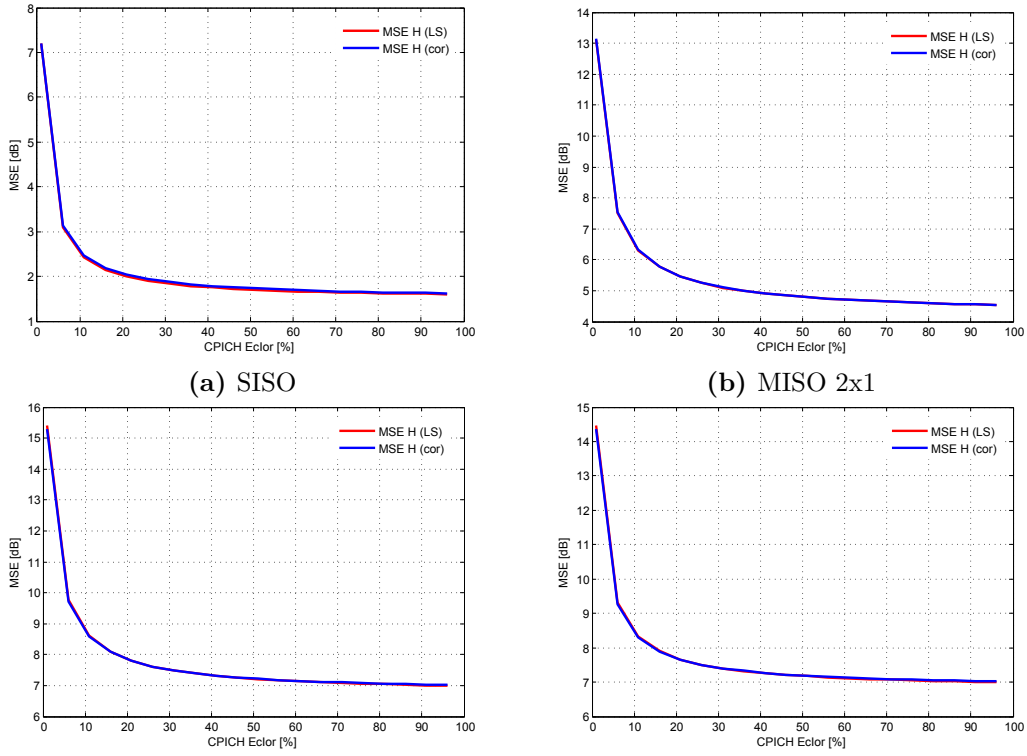


**(a)** SISO **(b)** MISO 2x1

**(c)** MIMO 2x2 TxAA **(d)** MIMO 2x2 D-TxAA

**Figure 4.5.:** MSE channel coefficients

of the channel coefficients, again for a particular $\mathrm{CPICH}_{E_c/I_0}$ and channel estimator algorithm.

### 4.3.3. Modeling the effects of CPICH

In principle, in a real system, the UE would accomplish the equalization using the channel estimated coefficients provided by the channel estimator. In the case of our link-level simulator, the equalizer shows the following structure

$$\mathbf{f}^{(\mathrm{k})} = \sigma_s^2 \left( \hat{\mathbf{H}}_w \mathbf{R}_{ss} \hat{\mathbf{H}}_w^{\mathrm{H}} + \mathbf{R}_{vv} \right)^{-1} \hat{\mathbf{H}}_w \mathbf{e}_{\tau_k, 2(L_\mathrm{h}+L_\mathrm{f}-1)}. \tag{4.14}$$

where the vector $\mathbf{e}_{\tau_k, 2(L_\mathrm{h}+L_\mathrm{f}-1)}$ is a zero vector of length $2(L_\mathrm{h}+L_\mathrm{f}-1)$ with a single one at position

$$\tau_k = \tau + (k-1)(L_\mathrm{h}+L_\mathrm{f}-1) \quad k = 1 \ldots K, \tag{4.15}$$

and $\hat{\mathbf{H}}_w \triangleq \hat{\mathbf{H}}(\mathbf{W} \otimes \mathbf{I}_{L_\mathrm{h}+L_\mathrm{f}-1})$.

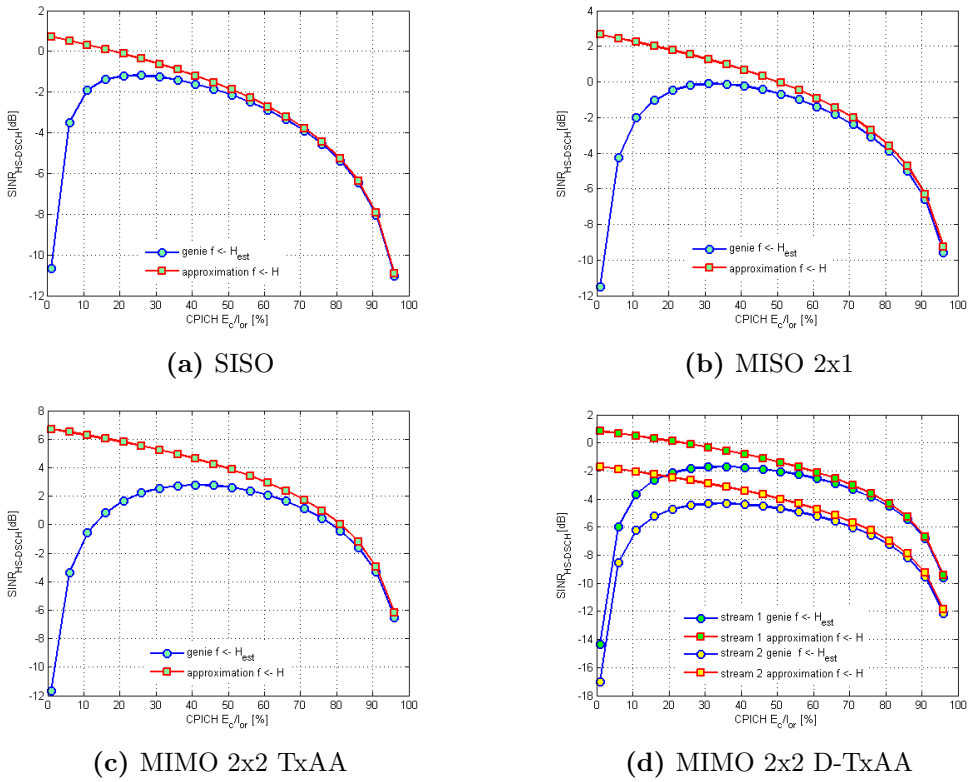


**(a)** SISO **(b)** MISO 2x1

**(c)** MIMO 2x2 TxAA **(d)** MIMO 2x2 D-TxAA

**Figure 4.6.:** Effect of CPICH in the current model and LS estimator

The solution of including a channel estimator in the calculation of the *fading parameters* is not desired, for the reason that it would increase the computational complexity of the system-level simulator.

Since we do not want to increase the computational complexity, we have to find out how to incorporate the estimated channel without directly utilizing channel estimators. Our proposal is based on considering the estimated channel matrix $\hat{\mathbf{H}}$ as the true channel matrix $\mathbf{H}$ and a matrix $\mathbf{H}_\Delta$ representing the channel estimation error. This can be express as

$$\hat{\mathbf{H}} = \mathbf{H} + \mathbf{H}_\Delta. \tag{4.16}$$

The matrix $\mathbf{H}_\Delta$ is constructed like the channel matrix $\mathbf{H}$ (in 3.10, or in 4.1 if we use the structure of the link-measurement model). The non-zero elements of $\mathbf{H}_\Delta$ are assumed to be a i.i.d. Gaussian with 0 mean and a variance equal to the MSE of the channel estimator, that as it has been shown before depends on the noise term and the estimator itself. Thus, we can say that

$$\mathrm{Var}\{\mathbf{H}_\Delta\} = f(\text{estimator algorithm}, \mathrm{CPICH}_{E_c/I_0}) \tag{4.17}$$

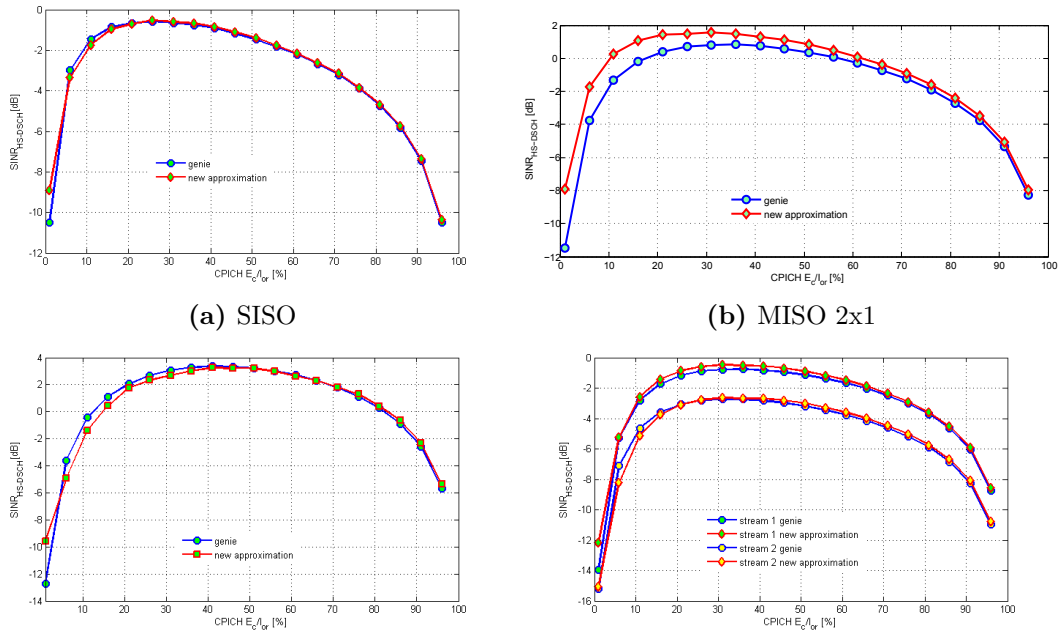


**(a)** SISO **(b)** MISO 2x1

**(c)** MIMO 2x2 TxAA **(d)** MIMO 2x2 D-TxAA

**Figure 4.7.:** Model validation and LS estimator

Hence we can say that the ST-MMSE equalizer in (4.14), becomes

$$\mathbf{f}^{(\mathrm{k})} = \sigma_s^2 \Big( (\mathbf{H}_w + \mathbf{H}_{w\Delta}) \mathbf{R}_{ss} (\mathbf{H}_w + \mathbf{H}_{w\Delta})^{\mathrm{H}} + \mathbf{R}_{vv} \Big)^{-1} (\mathbf{H}_w + \mathbf{H}_{w\Delta}) \mathbf{e}_{\tau_k, 2(L_\mathrm{h}+L_\mathrm{f}-1)}. \quad (4.18)$$

This solution enables the possibility to have a set of pre-calculated MSE curves which can be used to model the effects of the CPICH channel in a system-level simulator without increasing the computational complexity in excess because only a scalar product and a sum of matrix have to be performed during the generation of the fading parameters.

### 4.3.4. Validation of the enhanced model

We have conducted a set of validations of the new model, for different $\mathrm{CPICH}_{E_c/I_0}$, the results can be seen in Figure 4.7. Although the matrix $\mathbf{H}_{w\Delta}$ depends on the variance of a random variable, it can be seen that the fitting is very good.

# 5. CPICH Power Optimization

This chapter covers the analysis of the CPICH, and the optimization of the power allocated to this channel. The outline is as follows: Section 5.1 contains the analysis of the CPICH showing its main effects due to power variation. The simulation methodology utilized which leads to obtain the optimization of the CPICH power is explained in Section 5.2. Finally the simulation results are presented in Section 5.3.

## 5.1. Importance of CPICH power optimization

In HSDPA, as in UMTS, channel estimation is accomplished through the use of a signaling channel. The CPICH is this signaling channel. It is a fixed rate downlink physical channel that carries a pre-defined bit sequence. Apart from being utilized for the channel estimation in the HS-DSCH, the CPICH also provides the channel estimation reference for common channels.

The measurements of the CPICH are used in the cell selection, cell reselection and handover procedures. The UEs scan for the CPICH signals continuously and measure the received level of chip energy to interference plus noise density ratio ($E_c/I_0$) of all pilot signals they can detect. $I_0$ denotes the total received power density, including signal and interference, as measured at the UE antenna connector. In order to keep a mobile referenced to a cell, the $E_c/I_0$ at the mobile terminal must exceed a minimum threshold at all times. The $E_c/I_0$ ratio can be described as

$$\mathrm{CPICH}_{E_c/I_0} = \frac{\frac{P_{\mathrm{CPICH}}}{L_p}}{\sum_{i=1}^{numBS} \frac{P_{\mathrm{TX},i}}{L_p i} + I_{\mathrm{intra}} + N_0}, \tag{5.1}$$

where $P_{\mathrm{CPICH}}$ is the CPICH power of the cell we are measuring, $L_p$ is the overall path loss to the best server, $P_{\mathrm{TX},i}$ is the total transmit power by the base station $i$, $L_{pi}$ is the overall path loss to base station $i$, $I_{\mathrm{intra}}$ is the intracell interference, due to loss of orthogonality between channelisation codes, $N_0$ is the thermal noise of the UE and $numBS$ is the number of base stations in the network [25].

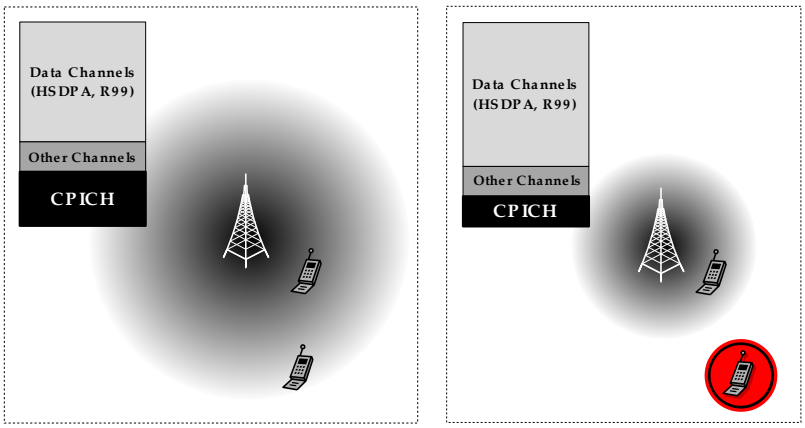


**Figure 5.1.:** Cell resizing effect due to CPICH power variation

The cell with the highest CPICH level at the UE is selected as the *serving cell*. As a consequence by adjusting the CPICH power level, the cell load can be balanced between different cells. Reducing the CPICH power causes part of the terminals to hand over to other cells, while increasing it invites more terminals to hand over to the cell, as well as to make their initial access to the network in that cell. This effect is depicted in Figure 5.1.

If a mobile terminal is unable to clearly receive one dominant CPICH signal, due to interference or coverage problems and therefore the terminal can not perform an effective estimation of the channel, the result is likely to be dropped calls, failed initiations, poor voice quality and/or data throughput. Figure 4.5d shows the MSE of the channel coefficients for a MIMO 2x2 TxAA link. It can be observed that the MSE increases when the amount of power allocated to the CPICH decreases, in other words, the less power assigned to the pilot channel the worse estimation of the channel.

Nevertheless, the more power is spent for pilot signalling, the less power is left to serve the user traffic. Excessive pilot power can easily take too large proportion of the total available transmit power, so that not enough power is left for traffic channels. Even considering the hypothetical case of having infinite power in both channels, the increase of the pilot channel would be beneficial just before reaching an upper limit. One of the limiting factors is the loss of orthogonality between spreading codes.

Another limiting factor, which we do not take into account for our analysis, that is produced due to too high values of CPICH power is called *pilot pollution*. Hearing equal powered CPICH signals or multiple strong CPICH with their multipath components causes pilot pollution. One of the possible consequences of pilot pollution is

| Parameter | Value |
|---|---|
| total power available at Base Station | 20 W |
| distance between Base Stations | 1000 m |
| antenna pattern | 3gpp 25.996 |
| path loss model | urban micro, COST231 Walfish-Ikegami |
| number of cells | 19 |
| number of Sectors/cell | 3 |
| transmitter frequency | 2 GHz |
| receiver noise figure | 9 dB |

**Table 5.1.:** Simulation scenario

that a UE may change the best serving cell continuously due to slow faded CPICH signals, increasing the signaling load in the network by causing additional cell reselection messages.

## 5.2. Simulation methodology

To ascertain the optimal CPICH power in a network we have used a basic network simulator (Section 5.2.1) that provides the overall inter-cell interference plus thermal noise in the UE ($I_{all}$) for a particular scenario. This $I_{all}$ depends basically on the scenario parameters and the position of the UE inside the cell. Consider one UE with a particular $I_{all}$ associated, this overall interference term is then introduced in the basic MIMO HSDPA link-level simulator (Section 3) and with it we derive the CPICH power value that maximizes the HS-DSCH SINR. In any case, this value will be only optimal for this particular user, so the process is repeated for a uniform grid inside one sector for the purpose of obtaining a uniform number of maximums inside a sector which allows us to calculate the optimal CPICH power of the cell by averaging.

### 5.2.1. Pre-equalization SINR

In fact, the simulator, which we use to obtain the overall interference term ($I_{all}$), is designed to calculate a pre-equalization SINR of set of points in a defined area for a given base station transmission power of the sector $i$, $P_{\mathrm{TX},i}$, and a set of parameters that define a uniform HSDPA network. In our case this SINR in particular spot inside the defined area corresponds to Equation (5.1) when $I_{\mathrm{intra}}$ is set to 0, from now on we will refer to this pre-equalization SINR as $\widehat{\mathrm{CPICH}}_{E_c/I_0,s}$. Table 5.1 shows the parameters that have been used in the simulations.

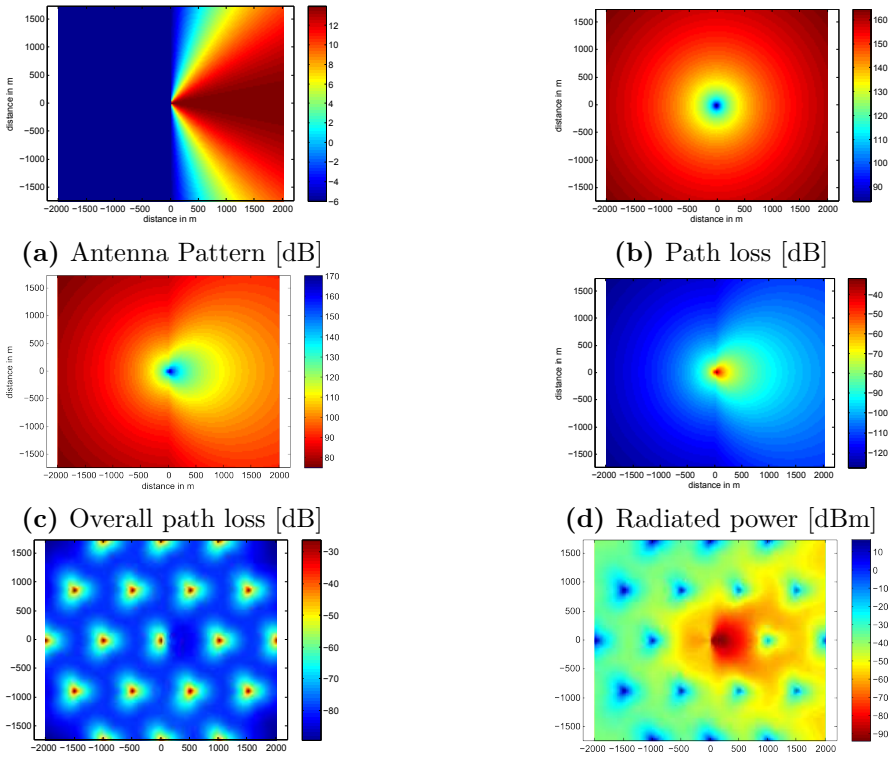


**(a)** Antenna Pattern [dB]

**(b)** Path loss [dB]

**(c)** Overall path loss [dB]

**(d)** Radiated power [dBm]

**(e)** Overall interference [dB]

**(f)** pre-equalized SNR [dBm]

**Figure 5.2.:** Path loss figures

The $\widehat{\text{CPICH}}_{E_c/I_0,s}$, as it is calculated in the simulator, for a particular spot is described as

$$\widehat{\text{CPICH}}_{E_c/I_0,s} = \frac{\frac{P_{\text{TX},i}}{L_p}}{\sum_{k=1}^{numBS} \frac{P_{\text{TX},k}}{L_{kp}} + N_0} \tag{5.2}$$

where $s$ is the spot index, $N_0$ is the thermal noise at the receiver, $L_{ip}$ is the overall link loss between the base station at cell $i$ and the user at the position $p$, and it is calculated as follows

$$L_{ip} = l_{ip}/G_{ip} \tag{5.3}$$

where $l_{ip}$ is the path loss (Figure 5.2b) calculated using COST231 Walfish-Ikegami model for urban micro environments (see Section 2.2.3) and $G_{ip}$ is the antenna gain (Figure 5.2b) which depends on the antenna pattern defined in [26]. The resulting overall path loss for the defined area can be seen in Figure 5.2c.

The radiated power of the target sector, $\frac{P_{\text{TX},i}}{L_p}$, can be seen in Figure 5.2d.

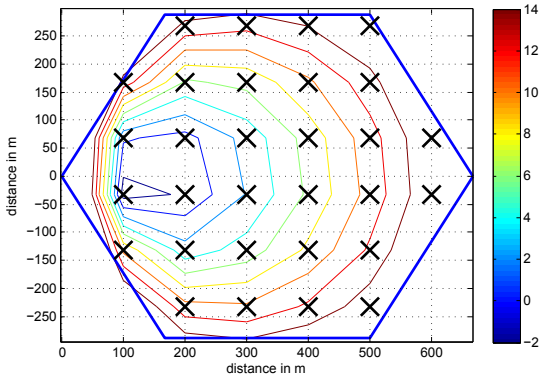


**Figure 5.3.:** $I_{all}$ [dBW] of the target sector

The sum of the inter-cell interference and thermal noise can be seen in Figure 5.2e where each dot represents one base station and the target base station is situated at the position (0,0). The resulting $\widehat{\text{CPICH}}_{E_c/I_0}$ in the target sector for each spot is depicted in Figure 5.2f.

The channel in the basic MIMO HSDPA link-level simulator is normalized, it means that the path loss term must be included in the interference term. The noise term in this case includes the inter-cell interference and the thermal noise in the receiver. Once this have been considered the $I_{all}$ for a specific spot that will be inserted in the link-level simulator can be easily derived from (5.2) and becomes

$$I_{all} = L_p \cdot (I_{inter} + N_0) \tag{5.4}$$

where $I_{inter} = \sum_{k=1}^{numBS} \frac{P_{\text{TX},k}}{L_{kp}}$. Figure 5.3 shows the total number of spots that have been considered inside the target cell. Every cross has a different $I_{all}$ that will be entered in the link-level simulator.

### 5.2.2. HS-DSCH SINR optimization

Our approach considers the optimization of the power allocated to the CPICH when the SINR of the data channel (HS-DSCH) is maximal. Thus the cost function is

$$\left(\frac{E_c}{I_{or}}\right)_{\text{CPICH},opt} = \underset{\left(\frac{E_c}{I_{or}}\right)_{\text{CPICH}}}{\text{argmax}} \ \text{SINR}_{\text{HS-DSCH},s} \tag{5.5}$$

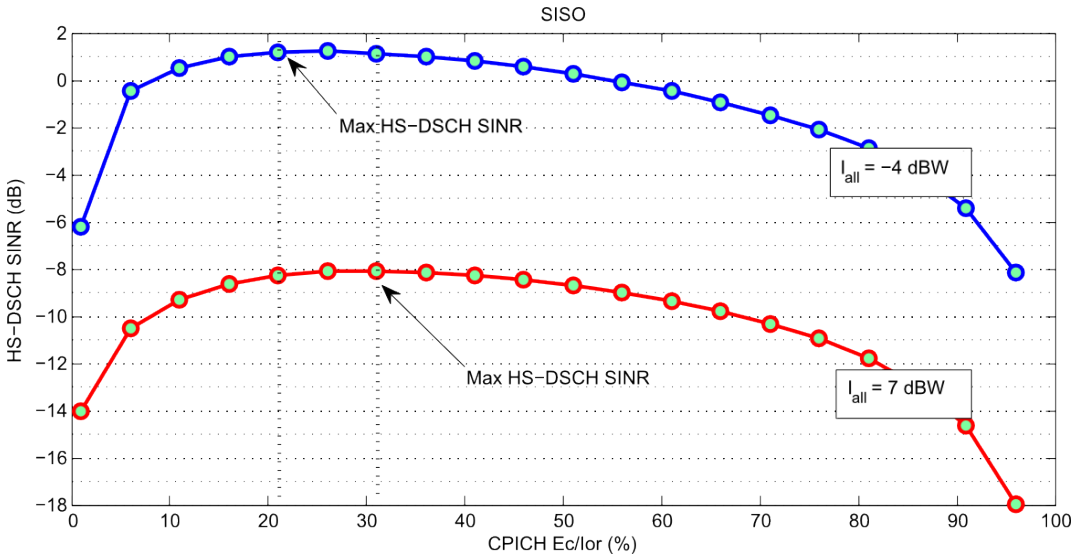


**Figure 5.4.:** $I_{all}$ Comparison

where $\text{SINR}_{\text{HS-DSCH},s}$ is the SINR in the data channel and the subindex $s$ indicates the spot position and therefore the $I_{all}$ associated. $\left(\frac{E_c}{I_{or}}\right)_{\text{CPICH}}$ is the power allocated to the CPICH as a fraction of the total transmission power $I_{or}$.

The procedure that leads to obtain the optimal point is the following:

1. Insert the ($I_{all}$) of a particular spot (see Figure 5.3), which has previously been acquired with the use of the pre-equalization SINR simulator, into the basic MIMO HSDPA link-level simulator.

2. Define $\text{SINR}_{\text{HS-DSCH},s}$ as a function of $\left(\frac{E_c}{I_{or}}\right)_{\text{CPICH}}$. Figure 5.4 shows an example with two functions in SISO transmission, each one is defined for a different $I_{all}$. It is important to emphasize that the base station transmitted power remains constant over the curve, in other words, an increase of the CPICH transmitted power infers a decrease of the HS-DSCH transmitted power, and vice versa.

3. Find the maximal $\text{SINR}_{\text{HS-DSCH},s}$ of the function, and its $\left(\frac{E_c}{I_{or}}\right)_{\text{CPICH}}$ associated. Note that the maximal of the function also changes with the change of the overall interference term.

4. Repeat the process for every spot inside the target sector.

Once the set of maximal $\text{SINR}_{\text{HS-DSCH},s}$, thus the optimal $\left(\frac{E_c}{I_{or}}\right)_{\text{CPICH}}$ values associated to them are found, we proceed to average the optimal $\left(\frac{E_c}{I_{or}}\right)_{\text{CPICH}}$ for the target

sector as follows. Suppose we have $\mathcal{S}$ spots in the target sector, in the single stream case the optimal value is originated from

$$Optimal \left(\frac{E_c}{I_{or}}\right)_{\text{CPICH}} = \frac{1}{\mathcal{S}} \sum_{s=0}^{\mathcal{S}} \underset{\left(\frac{E_c}{I_{or}}\right)_{\text{CPICH}}}{\text{argmax}} \text{SINR}_{\text{HS-DSCH},s} \tag{5.6}$$

In the case of double stream, the optimization is done independently per stream. Nevertheless, we see that both results are quite similar and decide to obtain the optimal by averaging both streams optimal values.

## 5.3. Simulation results

In this section we present the results of the optimal CPICH power that maximizes $\text{SINR}_{\text{HS-DSCH}}$, for each transmission scheme supported by our basic MIMO HSDPA link-level simulator. The configuration of the link-level simulator is done according to Table 5.2, and the parameters concerning the network are defined according to Table 5.1.

Figures 5.5 - 5.8 show the optimal CPICH transmission power for each spot according to the scenario specified for the SISO, MISO 2x1, MIMO TxAA and MIMO D-TxAA, respectively, for a Pedestrian B channel model and considering in the case of double stream the averaging of the results. Note that an increase of the CPICH power is required when the number of antennas increases, this effect is due to the increase in complexity of the channel. This extra complexity of the channel has a negative effect on the channel estimation which needs more help in terms of power to perform better. Table 5.3 sums up the results.

We have performed the simulation for Pedestrian A and Pedestrian B channel model. Pedestrian B (18 chips) is a very large channel when compared to Pedestrian A (3 chips). The optimal CPICH power when Pedestrian B is utilized is higher than when Pedestrian A is used, again, this is due to the difference in complexity of the channel. In the case of Pedestrian B the equalizer perform worse, which leads to an increase of the CPICH power to obtain the maximal data SINR.

However, the maximal data SINR is similar over a large range of values (See Figure 5.4. Thus the selection of the optimal CPICH power is actually only critical in a particular range, which is the range closer to the minimal CPICH power, where the slope is more pronounced.

| Parameter | Value |
|---|---|
| total power available at Base Station $I_{or}$ | 20 W |
| supported Transmission schemes | SISO, MISO, MIMO TxAA & D-TxAA |
| antenna utilization | 2x1, 2x2 |
| number of transmitted packets | 500 |
| equalizer span $L_{\mathrm{f}}$ | 30 chips |
| equalizer delay $\tau$ | 15 chips |
| transmitter frequency | 2 GHz |
| channel estimator | LS Estimator |
| channel model | ITU PedA, PedB |
| user mobility | 3 km/h |
| UE receiver type | ST-MMSE |
| beamforming delay $d_{bf}$ | 4 packets |
| utilized spreading codes for HS-DSCH | 15 |
| HS-DSCH modulation | 4-QAM |

**Table 5.2.:** link-level simulation parameters

| Transmission scheme | PedA Optimal CPICH | PedB Optimal CPICH |
|---|---|---|
| SISO | 4.16 W | 7.00 W |
| MISO 2x1 | 4.40 W | 7.93 W |
| MIMO 2x2 TxAA | 4.86 W | 8.53 W |
| MIMO 2x2 D-TxAA | 5.78 W | 8.81 W |

**Table 5.3.:** CPICH power optimization results

## 5.4. Conclusion

The optimal CPICH power obtain in this chapter is far from the one used in a real network, usually set to 5-10% of the total transmission power of the base station. The main reason is that pilot pollution is not considered, in any case the cost function utilized shows the effect of the CPICH power variation in each transmission scheme and sets the basis to develop new studies able to fit the real networks more accurately.

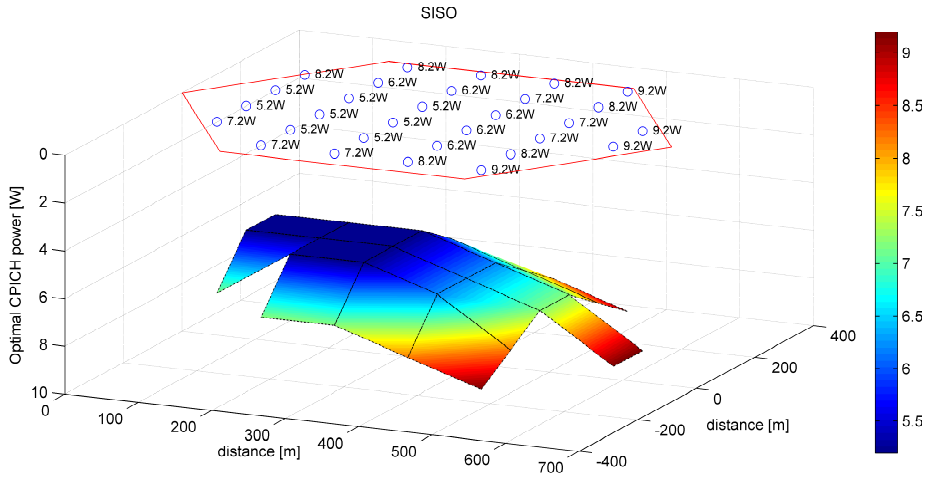


**Figure 5.5.:** SISO

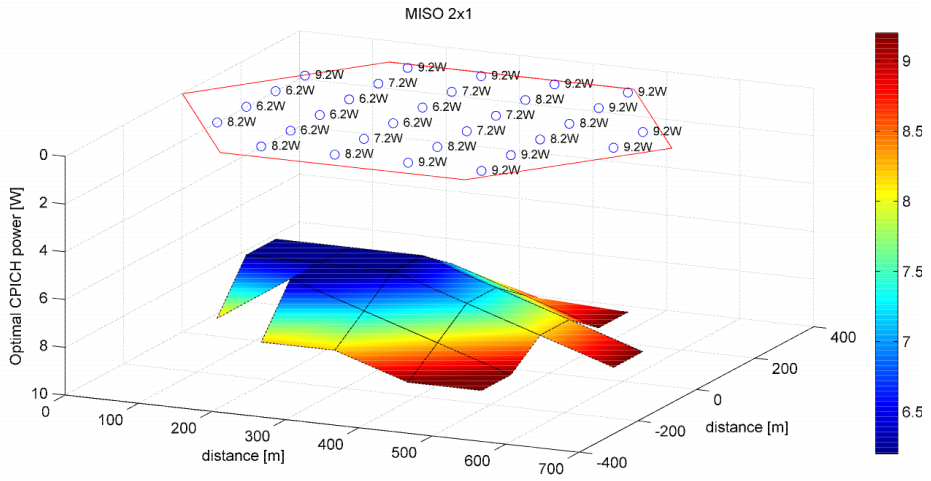


**Figure 5.6.:** MISO 2x1

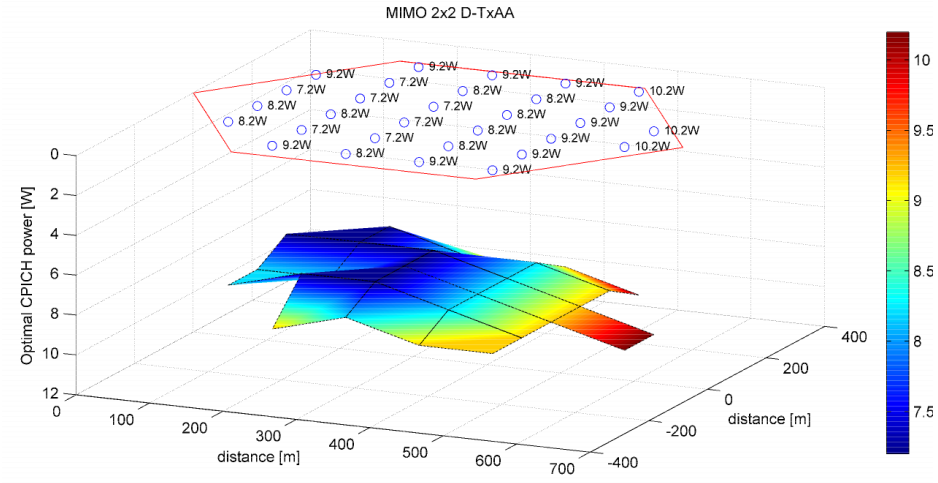


**Figure 5.7.:** MIMO 2x2 TxAA

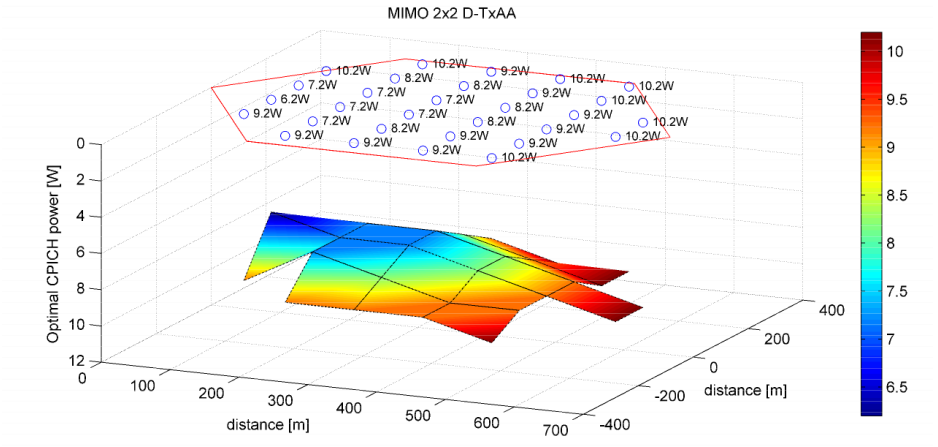


**Figure 5.8.:** MIMO 2x2 D-TxAA

# A. Appendix

## A.1. Channelisation Codes

The utilized channelisation codes are OVSF codes that preserve the orthogonality between a user's different physical channels. The OVSF codes can be defined using the code tree of Figure A.1 [27].

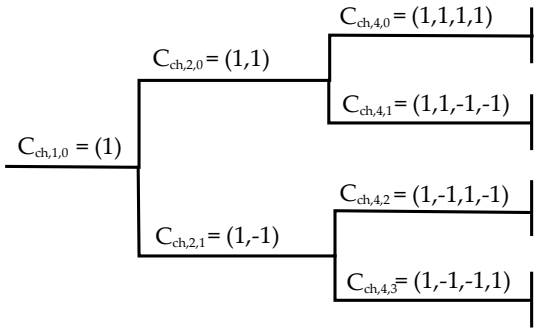


**Figure A.1.:** Code-tree for generation of OVSF codes

In Figure A.1, the channelisation codes are uniquely described as $C_{ch,SF,k}$, where SF is the spreading factor of the code and $k$ is the code number, $0 \leq k \leq SF - 1$.

Each level in the code tree defines channelisation codes of length SF, corresponding to a spreading factor of SF in Figure A.1.

The generation method for the channelisation code is defined as:

$$C_{ch,1,0} = 1,$$

$$\begin{bmatrix} C_{ch,2,0} \\ C_{ch,2,1} \end{bmatrix} = \begin{bmatrix} C_{ch,1,0} & C_{ch,1,0} \\ C_{ch,1,0} & -C_{ch,1,0} \end{bmatrix} = \begin{bmatrix} 1 & 1 \\ 1 & -1 \end{bmatrix}$$

$$\begin{bmatrix} C_{ch,2^{(n+1)},0} \\ C_{ch,2^{(n+1)},1} \\ C_{ch,2^{(n+1)},2} \\ C_{ch,2^{(n+1)},3} \\ \vdots \\ C_{ch,,2^{(n+1)}2^{(n+1)}-2} \\ C_{ch,,2^{(n+1)}2^{(n+1)}-1} \end{bmatrix} = \begin{bmatrix} C_{ch,2^n,0} & C_{ch,2^n,0} \\ C_{ch,2^n,0} & -C_{ch,2^n,0} \\ C_{ch,2^n,1} & C_{ch,2^n,1} \\ C_{ch,2^n,1} & -C_{ch,2^n,1} \\ \vdots & \vdots \\ C_{ch,2^n,2^n-1} & C_{ch,2^n,2^n-1} \\ C_{ch,2^n,2^n-1} & -C_{ch,2^n,2^n-1} \end{bmatrix}$$

The leftmost value in each channelisation code word corresponds to the chip transmitted first in time.

## A.2. Scrambling

The scrambling code sequences are constructed by combining two real sequences into a complex sequence [27]. Each of the two real sequences are constructed as the position wise modulo 2 sum of 38400 chip segments of two binary $m$-sequences generated by means of two generator polynomials of degree 18. The resulting sequences thus constitute segments of a set of Gold sequences. The scrambling codes are repeated for every 10 ms radio frame. Let $x$ and $y$ be the two sequences respectively. The $x$ sequence is constructed using the primitive (over GF(2)) polynomial $1+X^7+X^{18}$ . The $y$ sequence is constructed using the polynomial $1 + X^5 + X^7 + X^10 + X^{18}$.

The sequence depending on the chosen scrambling code number $n$ is denoted $z_n$, in the sequel. Furthermore, let $x(i)$, $y(i)$ and $z_n(i)$ denote the $i$:th symbol of the sequence $x$, $y$, and $z_n$, respectively. The $m$-sequences $x$ and $y$ are constructed as:

Initial conditions:

- $x$ is constructed with $x(0) = 1, x(1) = x(2) = \ldots = x(16) = x(17) = 0$.
- $y(0) = y(1) = \ldots = y(16) = y(17) = 1$

Recursive definition of subsequent symbols:

- $x(i + 18) = x(i + 7) + x(i) \bmod 2,\ i = 0, \ldots, 2^{18} - 20$.
- $y(i + 18) = y(i + 10) + y(i + 7) + y(i + 5) + y(i) \bmod 2,\ i = 0, \ldots, 2^{18} - 20$.

The $n$:th Gold code sequence $z_n$, $n = 0, 1, 2, \ldots, 2^{18}-2$, is then defined as:

- $z_n(i) = x((i + n) \bmod (2^{18} - 1)) + y(i) \bmod 2,\ i = 0, \ldots, 2^{18} - 2$.

These binary sequences are converted to real valued sequences $Z_n$ by the following transformation:

$$Z_n(i) = \begin{cases} +1 & \text{if } Z_n(i) = 0 \\ -1 & \text{if } Z_n(i) = 1 \end{cases} \text{ for } i = 0, 1, \ldots, 2^{18} - 2$$

Finally, the $n$:th complex scrambling code sequence $S_{dl,n}$ is defined as:

- $S_{dl,n}(i) = Z_n(i) + jZ_n((i + 131072) \bmod (2^{18} - 1)),\ i = 0, 1, \ldots, 38399.$

Note that the pattern from phase 0 up to the phase of 38399 is repeated.

# Bibliography


[1] H. Holma and A. Toskala, *HSDPA/HSUPA for UMTS*. The Atrium, Southern Gate, Chichester, West Sussex PO19 8SQ, England: John Wiley & Sons, Ltd, 2006.

[2] 3GPP, *Technical Specification Group Radio Access Network; Multiple Input Multiple Output in UTRA (Tech. Spec. 25.876 V7.0.0)*, release 7 ed., March 2007.

[3] 3GPP, *Technical Specification Group Radio Access Network; Physical channels and mapping of transport channels onto physical channels (FDD) (Tech. Spec. 25.211 V8.2.0)*, release 7 ed., September 2008.

[4] M. of WINNER, "Assessment of advanced beamforming and MIMO technologies," Tech. Rep. Tech. Rep IST-2003-507581 D.2.7 v1.0, WINNER, 2003.

[5] M. Wrulich, S. Eder, I. Viering, and M. Rupp, "Efficient link-to-system level model for MIMO HSDPA," *GLOBECOM Workshops IEEE*, 2008.

[6] "www.3gpp.org."

[7] J. Ramis, "Mobile communication networks lecture notes." Lecture slides, available online: http://dmi.uib.es/ jramis/, University of Balearic Island, 2005.

[8] G. L. Stüber, *Principles of Mobile Communication*. Kluwer Academic Publishers, 2nd ed., 2001.

[9] H. Holma and A. Toskala, *WCDMA for UMTS*. The Atrium, Southern Gate, Chichester, West Sussex PO19 8SQ, England: John Wiley & Sons, Ltd, 2004.

[10] B. Sklar, "Rayleigh fading channel in mobile digital communication systems part I: Characterization," *IEEE Communications Magazine*, 1997.

[11] COST 231, *Digital mobile radio towards future generation systems*.

[12] Qualcomm, "Release 7 hspa+ for mobile broadband evolution." available online: http://hspa.gsmworld.com/upload/news/files/10122007082416.pdf, 2007.

[13] P. Soler, "MIMO en sistemes hiperlan/2 i ieee 802.11a.," Master's thesis, University of Balearic Island, 2007.

[14] S. Geirhofer, C. Mehlführer, and M. Rupp, "Design and real-time measurement of HSDPA equalizers," *SPAWC*, 2005.

[15] E. Zacarías, "Adaptive transmit beamforming with closed loop feedback in MIMO systems," *Postgraduate course in Radio Communications*, 2004.

[16] Y. Rosa and C. Xiao, "Simulation models with correct statistical properties for rayleigh fading channels," *IEEE TRANSACTIONS ON COMMUNICATIONS*, vol. 51, June 2003.

[17] ITU-R, "Recommendation itu-r m.1225: Guidelines for evaluation of radio transmission technologies for imt-2000," tech. rep., Tech.Rep., 1997.

[18] 3GPP, *Technical Specification Group Radio Access Network; User Equipment (UE) radio transmission and reception (FDD) (Tech. Spec. 25.101 V7.14.0)*, release 7 ed., December 2008.

[19] C. Mehlführer, M. Wrulich, and M. Rupp, "Intra-cell interference aware equalization for TxAA HSDPA," *Wireless Pervasive Computing*, 2008.

[20] C. Mehlführer, S. Caban, and M. Rupp, "Measurement based evaluation of low complexity receivers for D-TxAA HSDPA," *EUPISCO*, 2008.

[21] C. Mehlführer and M. Rupp, "Novel tap-wise LMMSE channel estimation for MIMO WCDMA," *Global Telecommunications Conference*, 2008.

[22] S. M. Kay, *Fundamentals of statistical Signal Processing: Estimation Theory*, vol. 2. Prentice Hall, 1993.

[23] M. Wrulich and M. Rupp, "Computationally efficient MIMO HSDPA system-level evaluation," *EURASIP, WIRELESS COMMUNICATIONS AND NETWORKING*, August 2009.

[24] M. Wrulich, C. Mecklenbräuker, and J. Wehinger, "Upgrading methodology for MIMO system-level simulations," in *Wireless Evolution Beyond 3G*, ftw. C10, 2007.

[25] W. Karner, "Optimum default base station parameter settings for UMTS networks," Master's thesis, Technischen Universit¨at Wien, 2003.

[26] 3GPP, *Technical Specification Group Radio Access Network; Spatial channel model for Multiple Input Multiple Output (MIMO) simulations (Tech. Spec. 25.996 V6.1.0)*, release 6 ed., September 2003.

[27] 3GPP, *Technical Specification Group Radio Access Network; Spreading and modulation (FDD) (Tech. Spec. 25.213 V7.6.0)*, release 7 ed., September 2008.